J. Phase Equilib. Diffus. (2017) 38:509–542
DOI 10.1007/s11669-017-0546-7

Critical Systematic Evaluation and Thermodynamic Optimization of the Fe-RE System: RE = Gd, Tb, Dy, Ho, Er, Tm, Lu, and Y

Bikram Konar[1] · Junghwan Kim[1] · In-Ho Jung[1]

Submitted: 24 July 2016 / in revised form: 21 March 2017 / Published online: 17 April 2017

Abstract As the second part of the thermodynamic study of binary Fe-RE system, critical evaluations and optimizations of all available phase diagrams and thermodynamic data for the Fe-heavy RE (heavy RE = Gd, Tb, Dy, Ho, Er, Tm, Lu, and Y) systems were conducted to obtain reliable thermodynamic functions of all the phases in the systems. In the thermodynamic modeling of the heavy RE systems, systematic variations in the phase diagrams and thermodynamic properties such as the enthalpy of mixing in the liquid state and enthalpy of formation of solid compounds with the atomic number of lanthanide series were observed. These systematic trends were incorporated in the optimization of the Fe-heavy RE system to resolve inconsistencies between available experimental data and to estimate unknown thermodynamic properties. The systematic trends in thermodynamic properties of solid and liquid phases and phase diagram of the entire Fe-RE systems were summarized.

Keywords enthalpy of mixing · Fe-RE system · phase diagrams · rare-earth alloys and compounds · thermodynamic optimization

1 Introduction

Rare earth (RE) elements are used as important alloying elements for the applications to permanent magnets, electronics, and power industries. The addition of heavy-RE elements enhances the magnetic, electronic, optical and mechanical properties of alloys. Compounds of heavy-RE elements with other metals like Co, Fe, Ni etc. have unique properties of optical,[1] magnetic,[2] magnetocaloric effect,[3–5] magnetostriction[6] and electrical conductivity,[7] and electrocatalytic properties.[8,9] These properties make them valuable to the electronic, appliance, green technology, weapon and medical device manufacturing industry.[10,11] In addition, several studies[12–14] related to the use of RE elements in steel metallurgy as strong deoxidants, microstructure refining alloys, and inclusion modifiers have been performed.

Accurate thermodynamic properties and phase diagrams of alloys are indispensable for the development of alloy design and processing. In particular, CALPHAD type thermodynamic databases are widely used in such applications. The thermodynamic database can be developed through 'thermodynamic optimization' process involving critical and simultaneous evaluation of all thermodynamic and phase equilibrium data available from the literature. During optimization, the thermodynamic properties such as activity, enthalpy and entropy are considered along with phase diagram information. The discrepancy even between different types of experimental data is evaluated to comply with the thermodynamic principles. After a critical evaluation of the available experimental data, a self-consistent set of Gibbs energy equations for all phases in the given system was obtained to reproduce all reliable experimental data. This set of Gibbs equations can be used along with computer software containing the Gibbs energy minimizing routine like FactSage[15] to back calculate any phase equilibria, phase diagram and thermodynamic properties useful for new materials development and processing.

As part of the wide research program for the recycling of RE elements from waste RE magnets and electronic

✉ In-Ho Jung
in-ho.jung@mcgill.ca

[1] Department of Mining and Materials Engineering, McGill University, 3610 University St., Montreal, QC H3A 0C5, Canada

components,[16,17] and also to introduce RE elements in new Mg alloy development,[18] thermodynamic optimization of many binary and ternary RE elements containing systems was performed. In particular, to obtain an accurate thermodynamic description of binary RE-ME (ME = Fe, Sn, Mn, Si, Pb, Al, Mg, and Zn) systems, systematic and critical assessments of the thermodynamic and phase diagram data were performed. For example, we have already performed thermodynamic optimization for RE-Sn,[19,20] Mn,[21–23] Si,[24,25] Pb,[26] Al,[27,28] Mg,[29] and Zn.[30]

In our previous study[31] the critical evaluation and optimization of the Fe-light RE systems, where RE = La, Ce, Pr, Nd, and Sm, was performed. As the second part of the thermodynamic modeling study of the whole Fe-RE systems, the critical optimization of the Fe-heavy RE systems where RE = Gd, Tb, Dy, Ho, Er, Tm, Lu, and Y is presented in this study. As pointed out in many binary RE alloy systems,[16,21,23,25] the systematic trends in thermodynamic properties and phase diagram information are used to resolve existing inconsistency between experimental data and predict the unknown thermodynamic and phase diagram data.

2 Thermodynamic Models

The thermodynamic models for liquid and solid phases are the same as described in the previous work[31] for the Fe-light RE system. The modified quasichemical model (MQM) was used to describe the liquid solution in all binary systems. The model has been described in detail by Pelton et al.[32,33] which accounts for short-range ordering and gives a realistic thermodynamic description of liquid phase compared to that obtained from conventional simple random-mixing Bragg–Williams model.[32,33] The Gibbs energies of all pure elements were taken from SGTE database version 5.0.[34] The Gibbs energies of stoichiometric compounds were optimized based on available thermodynamic data such as heat capacity, enthalpy and entropy of formation at 298 K. If the heat capacities of stoichiometric compounds were not available, they were typically estimated using the Neumann–Kopp (N–K) rule.[35] If the entropies of the compounds were unknown, typically N–K rule was applied as the first approximation. In some instances, they were slightly adjusted based on the periodic trend along the RE series to reproduce the phase diagram of the system. Iron and most of the compounds in Fe-RE binary system have magnetic transitions involving the Néel or Curie temperature. The magnetic contribution (G_{Mag}) to the Gibbs energy of phase was described following an empirical relationship suggested by Inden[36] and modified by Hillert and Jarl.[37] The solid solutions, Fe-rich solution and RE-rich solution, appearing in a binary system were described by the Compound Energy Formalism (CEF)[38] with one sublattice (substitutional site) model which can be occupied by Fe and RE atom. The details of thermodynamic models can be found in the previous study[31] for the Fe-light RE systems.

3 Critical Evaluation and Thermodynamic Optimization

The crystal structures of the intermetallic phases considered in the present assessment are summarized in Table 1. The optimized thermodynamic model parameters of solid and liquid phases are presented in Table 2.

3.1 The Fe-Gd (Iron-Gadolinium) System

The thermodynamic assessment of Fe-Gd system was performed by Liu et al.,[39] Zinkevich et al.[40] and Konar.[41] Kubaschewski[42] and Okamoto[43] also reviewed this system. In all assessments, four intermetallic compounds (Gd_2Fe_{17}, Gd_6Fe_{23}, $GdFe_3$ and $GdFe_2$), bcc and fcc Fe solutions, bcc and hcp Gd solutions, and liquid (Liq) phase were considered.

The optimized calculated phase diagram of the Fe-Gd system is shown in Fig. 1 along with the experimental data.[44–50] The invariant reactions are summarized in Table 3. The phase diagram of the Fe-Gd system was first investigated by Novy et al.[50] Seven intermetallic phases, Gd_2Fe_3, $GdFe_2$, $GdFe_3$, Gd_2Fe_7, $GdFe_4$, $GdFe_5$ and Gd_2Fe_{17} along with five invariant reactions were reported by differential thermal analysis (DTA) technique and optical pyrometry. It can be said that this is very preliminary phase diagram of this system. Contrary to Novy et al.,[50] Copeland et al.[44] suggested three intermetallic phases $GdFe_9$, $GdFe_3$, and $GdFe_2$ with peritectic melting using thermal analysis (TA), optical microscopy (OM) and x-ray diffraction (XRD) phase analysis. The solidus and liquidus temperatures were determined by TA and visually by optical pyrometry. Savitskii et al.[45] investigated the phase diagram over the entire composition range with TA and equilibration technique followed by OM and XRD phase analyses and reported two compounds Gd_2Fe_{17} and $GdFe_2$ with peritectic melting. An eutectic reaction between Gd-rich phase and $GdFe_2$ was also reported at 0.72 mol fraction Gd (X_{Gd}) and 830 ± 7 °C. Later, Savitskii[46] reported four intermetallic phases Gd_2Fe_{17}, $GdFe_4$, $GdFe_3$, and $GdFe_2$ where all showed peritectic melting behaviors. In the review by Kubaschewski,[42] the phase diagram of the Fe-Gd system was proposed based on the experimental results of Copeland et al.[44] with the modification of peritectic melting of Gd_6Fe_{23} based on Savitskii et al.[46] and Burov et al.[48] Most recently, Atiq et al.[49]

Table 1 Summary of the crystal structures of the compounds in the heavy Fe-RE system

System	RE_2Fe_{17}			RE_6Fe_{23}			$REFe_3$			$REFe_2$		
	Crystal structure/space group		Prototype	Crystal structure/space group		Prototype	Crystal structure/space group		Prototype	Crystal structure/space group		Prototype
Fe-Gd	Rhombohedral	R3m	Th_2Zn_{17}[103]	Cubic	Fm3m	$Mn_{23}Th_6$[104]	Hexagonal	R3m	Ni_3Pu[115]	Cubic	Fd3m	$MgCu_2$[116]
Fe-Tb	Hexagonal	$P6_3/mmc$	Th_2Ni_{17}[63,103]	Cubic	Fm3m	$Mn_{23}Th_6$[104]	Hexagonal	R3m	Ni_3Pu[117]	Cubic	Fd3m	$MgCu_2$
Fe-Dy	Hexagonal	$P6_3/mmc$	Th_2Ni_{17}[103]	Cubic	Fm3m	$Mn_{23}Th_6$[118]	Hexagonal	R3m	Ni_3Pu[119]	Rhombohedral	R3m	distorted-$MgCu_2$[118]
Fe-Ho	Hexagonal	$P6_3/mmc$	Th_2Ni_{17}[120]	Cubic	Fm3m	$Mn_{23}Th_6$[121]	Hexagonal	R3m	Be_3Nb[75,115]	Cubic	Fd3m	$MgCu_2$[75]
Fe-Er	Hexagonal	$P6_3/mmc$	Th_2Ni_{17}[103]	Cubic	Fm3m	$Mn_{23}Th_6$[104]	Hexagonal	R3m	Ni_3Pu[117]	Cubic	Fd3m	$MgCu_2$[116]
Fe-Tm	Hexagonal	$P6_3/mmc$	Th_2Ni_{17}[122]	Cubic	Fm3m	$Mn_{23}Th_{63}$[104]	Hexagonal	R3m	Ni_3Pu[117]	Cubic	Fd3m	$MgCu_2$
Fe-Lu	Hexagonal	$P6_3/mmc$	Th_2Ni_{17}[123]	Cubic	Fm3m	$Mn_{23}Th_6$[104]	Orthorhombic[86]			Cubic	Fd3m	$MgCu_2$[116]
Fe-Y	Hexagonal	$P6_3/mmc$	Th_2Ni_{17}[103]	Cubic	Fm3m	$Mn_{23}Th_6$[104]	Hexagonal	R3m	Ni_3Pu[105]	Cubic	Fd3m	$MgCu_2$[106]

investigated the phase transformations in the Fe-rich side (less than 0.32 X_{Gd}) which were determined by DTA and diffusion couple technique. For the determination of phases in the diffusion couples, energy dispersive x-ray analysis (EDAX) was used. Atiq et al.[49] suggested a polymorphic transformation of the Gd_2Fe_{17} phase from rhombohedral (Th_2Zn_{17} type) to hexagonal (Th_2Ni_{17} type) structures at around 1215 ± 2 °C.

In the present optimization, four intermetallic phases $GdFe_2$, $GdFe_3$, Gd_6Fe_{23} and Gd_2Fe_{17}, and bcc, fcc and hcp Fe-Gd solutions were considered as solid phases. The $GdFe_9$ and $GdFe_4$ reported by Copeland et al.[44] and Savitskii[46] should be corresponding to Gd_2Fe_{17} and Gd_6Fe_{23}, respectively, according to more updated crystallographic information. The liquidus and solidus data by Savitskii et al.,[45,46] Burov et al.,[48] and Atiq et al.[49] were mainly considered in the present modeling. The polymorphic transformation of the Gd_2Fe_{17} phase reported by Atiq et al.[49] was not considered in the present study due to lack of information about the enthalpy of transformation. All the liquidus and peritectic transition temperatures in the Fe-Gd system were well reproduced in the present optimization within the experimental error. The peritectic reaction of Liq + Gd_2Fe_{17} → Gd_6Fe_{23} is calculated at 0.281 X_{Gd} in this study, which is slightly higher than the experimental value 0.28 X_{Gd} from Savitskii,[46] while the previous assessments calculated at about 0.235[39] and 0.210 X_{Gd}.[40] The other invariant reaction compositions are all calculated within experimental error ranges.

The solubility of Gd in bcc Fe and that of Fe in hcp Gd was reported by Savitskii et al.[46] and Burov et al.[48] as presented in Fig. 1(b) and (c). Savitskii et al.[46] reported the maximum solubility of Gd in bcc Fe to be 0.001 mol fraction of Gd at 800 °C and solubility of Fe in hcp Gd to be 0.006 mol fraction of Fe at 700 °C, respectively, using XRD measurement of quenched samples. Burov et al.[48] performed dilatometric analysis and determined the bcc Fe to fcc Fe transition and presented less than 0.001 mol fraction solubility of Gd in Fe in their diagram. On the contrary, Copeland et al.[44] reported no solubility of the solid phases from their optical metallographic observation of the sample. In this study, the data from Savitskii et al.[46] and Burov et al.[48] were accepted, and a regular solution parameter for a bcc Fe-Gd solution was determined to reproduce the solubility of Gd in bcc Fe. It should be noted that the eutectoid transition of bcc Fe → fcc Fe in the Fe-rich side determined by Atiq et al.[49] was also well reproduced as shown in Fig. 1(a). A temperature-dependent parameter for fcc Fe solution was necessary to reproduce the metatectic transition of bcc Fe → fcc Fe + Liq at 1381 °C, compared to 1389 ± 5 °C[49] as shown in Fig. 1(a). A temperature-dependent parameter for

Table 2 Optimized model parameters for the Fe-RE system (J mol^{-1} or J mol^{-1} K^{-1})

Liquid solution

Coordination numbers

i	j	Z_{ij}^{i}	Z_{ij}^{j}
Fe	Gd	6	6
Fe	Tb	6	6
Fe	Dy	6	6
Fe	Ho	6	6
Fe	Er	6	6
Fe	Tm	6	6
Fe	Lu	6	6
Fe	Y	6	6

$\Delta g_{\text{Fe-Gd}} = -7573.04 + 3.26\text{T} + (836.80 + 2.72\text{T})X_{\text{Fe-Fe}} + 3138.00X_{\text{Gd-Gd}}$

$\Delta g_{\text{Fe-Tb}} = -6652.56 + 2.72\text{T} - 1213.36X_{\text{Fe-Fe}} + 3.77\text{T}\ X_{Fe-Fe}^{2} - 7.53\text{T}\ X_{Fe-Fe}^{3} - 418.40X_{\text{Tb-Tb}}$

$\Delta g_{\text{Fe-Dy}} = -8368.00 + 4.60\text{T} - 6493.57X_{\text{Fe-Fe}} - 1673.60X_{\text{Dy-Dy}}$

$\Delta g_{\text{Fe-Ho}} = -9623.20 + 3.72\ \text{T} - 7322.00X_{\text{Fe-Fe}} + (1297.04 - 2.89\ \text{T})X_{\text{Ho-Ho}}$

$\Delta g_{\text{Fe-Er}} = -8786.40 + 1.76\text{T} - 6694.40X_{\text{Fe-Fe}} - 8368.00\ X_{Fe-Fe}^{3} + (8368.00 + 3.56\text{T})\ X_{Fe-Fe}^{5} - 4560.56X_{\text{Er-Er}}$

$\Delta g_{\text{Fe-Tm}} = -10{,}250.80 + 4.14\text{T} - 8786.40X_{\text{Fe-Fe}} - 5857.60\ X_{Fe-Fe}^{3} + (8786.40 + 3.26\text{T})\ X_{Fe-Fe}^{5} - 836.80X_{\text{Tm-Tm}}$

$\Delta g_{\text{Fe-Lu}} = -10{,}460.00 + 3.77\text{T} - 10{,}041.60X_{\text{Fe-Fe}} - 5857.60\ X_{Fe-Fe}^{3} + (9204.80 + 2.51\text{T})\ X_{Fe-Fe}^{5} - 2426.72X_{\text{Lu-Lu}}$

$\Delta g_{\text{Fe-Y}} = -11{,}506.00 + 5.23\text{T} + (2510.40 - 5.02\text{T})X_{\text{Fe-Fe}} + 3347.20X_{\text{Y-Y}}$

Solid solutions

fcc

$G_{fcc-Gd}^{o} = G_{hcp-Gd}^{o} + 1000$,[15] ${}^{0}\text{L}_{\text{Fe-Gd}} = 17{,}154.40 + 2.44764\ \text{T}$

$G_{fcc-Tb}^{o} = G_{hcp-Tb}^{o} + 100$,[15] ${}^{0}\text{L}_{\text{Fe-Tb}} = 7949.60 + 12.552\ \text{T}$

$G_{fcc-Dy}^{o} = G_{hcp-Dy}^{o} + 900$,[15] ${}^{0}\text{L}_{\text{Fe-Dy}} = 33{,}472.00$

$G_{fcc-Ho}^{o} = G_{hcp-Ho}^{o} + 1600$,[15] ${}^{0}\text{L}_{\text{Fe-Ho}} = 33{,}472.00$

$G_{fcc-Er}^{o} = G_{hcp-Er}^{o} + 2300$,[15] ${}^{0}\text{L}_{\text{Fe-Er}} = 33{,}472.00$

$G_{fcc-Tm}^{o} = G_{hcp-Tm}^{o} + 3100$,[15] ${}^{0}\text{L}_{\text{Fe-Tm}} = 33{,}472.00$

$G_{fcc-Lu}^{o} = G_{hcp-Lu}^{o} + 4100$,[15] ${}^{0}\text{L}_{\text{Fe-Lu}} = 33{,}472.00$

$G_{fcc-Y}^{o} = G_{hcp-Y}^{o} + 6000$,[15] ${}^{0}\text{L}_{\text{Fe-Y}} = 8995.60$

bcc

${}^{0}\text{L}_{\text{Fe-Gd}} = 18{,}828.00 + 1.8828\text{T}$

${}^{0}\text{L}_{\text{Fe-Tb}} = 3765.60 + 12.974\text{T}$

${}^{0}\text{L}_{\text{Fe-Dy}} = 33{,}472.00$

$G_{bcc-Ho}^{o} = G_{hcp-Ho}^{o} + 4380 - 2.4942T$,[15] ${}^{0}\text{L}_{\text{Fe-Ho}} = 29{,}288.00 + 8.368\text{T}$

${}^{0}\text{L}_{\text{Fe-Er}} = 33{,}472.00$

${}^{0}\text{L}_{\text{Fe-Tm}} = 33{,}472.00$

${}^{0}\text{L}_{\text{Fe-Lu}} = 33{,}472.00$

${}^{0}\text{L}_{\text{Fe-Y}} = -4184.00 + 20.08\text{T}$

hcp

${}^{0}\text{L}_{\text{Fe-Gd}} = 13{,}388.80 + 17.57\text{T}$

${}^{0}\text{L}_{\text{Fe-Tb}} = 23{,}514.08$

${}^{0}\text{L}_{\text{Fe-Dy}} = 29{,}288.00$

${}^{0}\text{L}_{\text{Fe-Ho}} = 50{,}208.00$

${}^{0}\text{L}_{\text{Fe-Er}} = 66{,}944.00$

${}^{0}\text{L}_{\text{Fe-Tm}} = 50{,}208.00$

${}^{0}\text{L}_{\text{Fe-Lu}} = 50{,}208.00$

${}^{0}\text{L}_{\text{Fe-Y}} = 25{,}187.68$

Compounds

$GdFe_2$

$\Delta H_{298}^{0} = -26{,}500.0$, $S_{298}^{0} = 109.380$

$C_{\text{p}} = 2 \times C_{\text{p}}$ (bcc Fe) + C_{p} (hcp Gd) + 12.31

T_C (Curie temperature) = 782 K, B_O (Magnetic moment) = $3.35\mu_B$ mol^{-1}, P factor = 0.28

Table 2 continued

$GdFe_3$	$\Delta H^0_{298} = -30{,}800.0$, $S^0_{298} = 141.400$
	$C_p = 3 \times C_p$ (bcc Fe) + C_p (hcp Gd) + 12.30789
	$T_C = 728$ K, $B_O = 1.6\mu_B$ mol^{-1}, P factor = 0.28
Gd_6Fe_{23}	$\Delta H^0_{298} = -171{,}650.0$, $S^0_{298} = 1035.000$
	$C_p = 23 \times C_p$ (bcc Fe) + $6 \times C_p$ (hcp Gd) + 73.85
	$T_C = 468$ K, $B_O = 14.8\mu_B$ mol^{-1}, P factor = 0.28
Gd_2Fe_{17}	$\Delta H^0_{298} = -47{,}600.0$, $S^0_{298} = 638.000$
	$C_p = 17 \times C_p$ (bcc Fe) + $2 \times C_p$ (hcp Gd) + 24.62
	$T_C = 472$ K, $B_O = 21.2\mu_B$ mol^{-1}, P factor = 0.28
$TbFe_2$	$\Delta H^0_{298} = -28{,}200.0$, $S^0_{298} = 116.800$
	$C_p = 2 \times C_p$ (bcc Fe) + C_p (hcp Tb) + 9.10
	$T_C = 704$ K, $B_O = 4.47\mu_B$ mol^{-1}, P factor = 0.28
$TbFe_3$	$\Delta H^0_{298} = -31{,}100.0$, $S^0_{298} = 157.900$
	$C_p = 3 \times C_p$ (bcc Fe) + C_p (hcp Tb)
	$T_C = 652$ K, $B_O = 3.13\mu_B$ mol^{-1}, P factor = 0.28
Tb_6Fe_{23}	$\Delta H^0_{298} = -173{,}000.0$, $S^0_{298} = 1155.500$
	$C_p = 23 \times C_p$ (bcc Fe) + $6 \times C_p$ (hcp Tb)
	$T_C = 574$ K, $B_O = 14.8\mu_B$ mol^{-1}, P factor = 0.28
Tb_2Fe_{17}	$\Delta H^0_{298} = -46{,}600.0$, $S^0_{298} = 688.000$
	$C_p = 17 \times C_p$ (bcc Fe) + $2 \times C_p$ (hcp Tb)
	$T_C = 408$ K, $B_O = 17.9\ \mu_B$ mol^{-1}, P factor = 0.28
$DyFe_2$	$\Delta H^0_{298} = -29{,}300.0$, $S^0_{298} = 118.100$
	$C_p = 2 \times C_p$ (bcc Fe) + C_p (hcp Dy) + 10.8
	$T_C = 635$ K, $B_O = 5.75\mu_B$ mol^{-1}, P factor = 0.28
$DyFe_3$	$\Delta H^0_{298} = -31{,}200.0$, $S^0_{298} = 162.700$
	$C_p = 3 \times C_p$ (bcc Fe) + C_p (hcp Dy)
	$T_C = 606$ K, $B_O = 3.97\mu_B$ mol^{-1}, P factor = 0.28
Dy_6Fe_{23}	$\Delta H^0_{298} = -175{,}800.0$, $S^0_{298} = 1183.200$
	$C_p = 23 \times C_p$ (bcc Fe) + $6 \times C_p$ (hcp Dy)
	$T_C = 534$ K, $B_O = 14.9\mu_B$ mol^{-1}, P factor = 0.28
Dy_2Fe_{17}	$\Delta H^0_{298} = -50{,}100.0$, $S^0_{298} = 702.000$
	$C_p = 17 \times C_p$ (bcc Fe) + $2 \times C_p$ (hcp Dy)
	$T_C = 371$ K, $B_O = 16.10\mu_B$ mol^{-1}, P factor = 0.28
$HoFe_2$	$\Delta H^0_{298} = -30{,}000.9$, $S^0_{298} = 122.100$
	$C_p = 2 \times C_p$ (bcc Fe) + C_p (hcp Ho) + 10.36
	$T_C = 635$ K, $B_O = 5.75\mu_B$ mol^{-1}, P factor = 0.28
$HoFe_3$	$\Delta H^0_{298} = -31{,}430.0$, $S^0_{298} = 166.300$
	$C_p = 3 \times C_p$ (bcc Fe) + C_p (hcp Ho)
	$T_C = 606$ K, $B_O = 3.97\mu_B$ mol^{-1}, P factor = 0.28
Ho_6Fe_{23}	$\Delta H^0_{298} = -178{,}052.0$, $S^0_{298} = 1217.000$
	$C_p = 23 \times C_p$ (bcc Fe) + $6 \times C_p$ (hcp Ho)
	$T_C = 534$ K, $B_O = 14.9\mu_B$ mol^{-1}, P factor = 0.28
Ho_2Fe_{17}	$\Delta H^0_{298} = -46{,}550.8$, $S^0_{298} = 714.000$
	$C_p = 17 \times C_p$ (bcc Fe) + $2 \times C_p$ (hcp Ho)
	$T_C = 371$ K, $B_O = 16.10\mu_B$ mol^{-1}, P factor = 0.28
$ErFe_2$	$\Delta H^0_{298} = -33{,}000.0$, $S^0_{298} = 128.270$
	$C_p = 2 \times C_p$ (bcc Fe) + C_p (hcp Er) + 5.41
	$T_C = 587$ K, $B_O = 4.85\mu_B$ mol^{-1}, P factor = 0.28

Table 2 continued

$ErFe_3$	$\Delta H^0_{298} = -33{,}033.2$, $S^0_{298} = 165.500$
	$C_p = 3 \times C_p$ (bcc Fe) + C_p (hcp Er) + 5.41
	$T_C = 552$ K, $B_O = 3.45\mu_B$ mol^{-1}, P factor = 0.28
Er_6Fe_{23}	$\Delta H^0_{298} = -178{,}052.2$, $S^0_{298} = 1208.000$
	$C_p = 23 \times C_p$ (bcc Fe) + $6 \times C_p$ (hcp Er) + 32.48
	$T_C = 494$ K, $B_O = 6.4\mu_B$ mol^{-1}, P factor = 0.28
Er_2Fe_{17}	$\Delta H^0_{298} = -46{,}500.0$, $S^0_{298} = 711.500$
	$C_p = 17 \times C_p$ (bcc Fe) + $2 \times C_p$ (hcp Er) + 10.83
	$T_C = 305$ K, $B_O = 17.1\mu_B$ mol^{-1}, P factor = 0.28
$TmFe_2$	$\Delta H^0_{298} = -33{,}700.0$, $S^0_{298} = 126.720$
	$C_p = 2 \times C_p$ (bcc Fe) + C_p (hcp Tm) + 5.26
	$T_C = 599$ K, $B_O = 2.61\mu_B$ mol^{-1}, P factor = 0.28
$TmFe_3$	$\Delta H^0_{298} = -33{,}400.0$, $S^0_{298} = 168.200$
	$C_p = 3 \times C_p$ (bcc Fe) + C_p (hcp Tm)
	$T_C = 537$ K, $B_O = 1.6\mu_B$ mol^{-1}, P factor = 0.28
Tm_6Fe_{23}	$\Delta H^0_{298} = -188{,}000.0$, $S^0_{298} = 1196.000$
	$C_p = 23 \times C_p$ (bcc Fe) + $6 \times C_p$ (hcp Tm)
	$T_C = 475$ K, $B_O = 18\mu_B$ mol^{-1}, P factor = 0.28
Tm_2Fe_{17}	$\Delta H^0_{298} = -47{,}100.0$, $S^0_{298} = 710.000$
	$C_p = 17 \times C_p$ (bcc Fe) + $2 \times C_p$ (hcp Tm)
	$T_C = 280$ K, $B_O = 20.4\mu_B$ mol^{-1}, P factor = 0.28
$LuFe_2$	$\Delta H^0_{298} = -35{,}300.0$, $S^0_{298} = 106.600$
	$C_p = 2 \times C_p$ (bcc Fe) + C_p (hcp Lu) + 2.8
	$T_C = 596$ K, $B_O = 2.93\mu_B$ mol^{-1}, P factor = 0.28
$LuFe_3$	$\Delta H^0_{298} = -33{,}900.0$, $S^0_{298} = 149.750$
	$C_p = 3 \times C_p$ (bcc Fe) + C_p (hcp Lu) + 2.8
	$T_C = 606$ K, $B_O = 3.97\mu_B$ mol^{-1}, P factor = 0.28
Lu_6Fe_{23}	$\Delta H^0_{298} = -205{,}000.0$, $S^0_{298} = 1045.300$
	$C_p = 23 \times C_p$ (bcc Fe) + $6 \times C_p$ (hcp Lu) + 16.8
	$T_C = 481$ K, $B_O = 43.9\mu_B$ mol^{-1}, P factor = 0.28
Lu_2Fe_{17}	$\Delta H^0_{298} = -56{,}500.0$, $S^0_{298} = 646.000$
	$C_p = 17 \times C_p$ (bcc Fe) + $2 \times C_p$ (hcp Lu) + 23.75
	$T_C = 268$ K, $B_O = 34.2\mu_B$ mol^{-1}, P factor = 0.28
YFe_2	$\Delta H^0_{298} = -6000.0$, $S^0_{298} = 114.800$
	$C_p = 2 \times C_p$ (bcc Fe) + C_p (hcp Y)
	$T_C = 542$ K, $B_O = 2.9\mu_B$ mol^{-1}, P factor = 0.28
YFe_3	$\Delta H^0_{298} = -7000.0$, $S^0_{298} = 150.1$
	$C_p = 3 \times C_p$ (bcc Fe) + C_p (hcp Y)
	$T_C = 569$ K, $B_O = 5.24\mu_B$ mol^{-1}, P factor = 0.28
Y_6Fe_{23}	$\Delta H^0_{298} = -25{,}000.0$, $S^0_{298} = 1118.000$
	$C_p = 23 \times C_p$ (bcc Fe) + $6 \times C_p$ (hcp Y)
	$T_C = 481$ K, $B_O = 43.1\mu_B$ mol^{-1}, P factor = 0.28
Y_2Fe_{17}	$\Delta H^0_{298} = -9800.0$, $S^0_{298} = 623.000$
	$C_p = 17 \times C_p$ (bcc Fe) + $2 \times C_p$ (hcp Y) + 58
	$T_C = 324$ K, $B_O = 32.9\mu_B$ mol^{-1}, P factor = 0.28

The Gibbs energies of liquid, hcp and bcc RE elements, and bcc, fcc and hcp Fe were taken from SGTE pure element database version 5.0.[34] The Gibbs energies of bcc Ho and fcc RE elements were taken from the FactSage FTLite database[15]

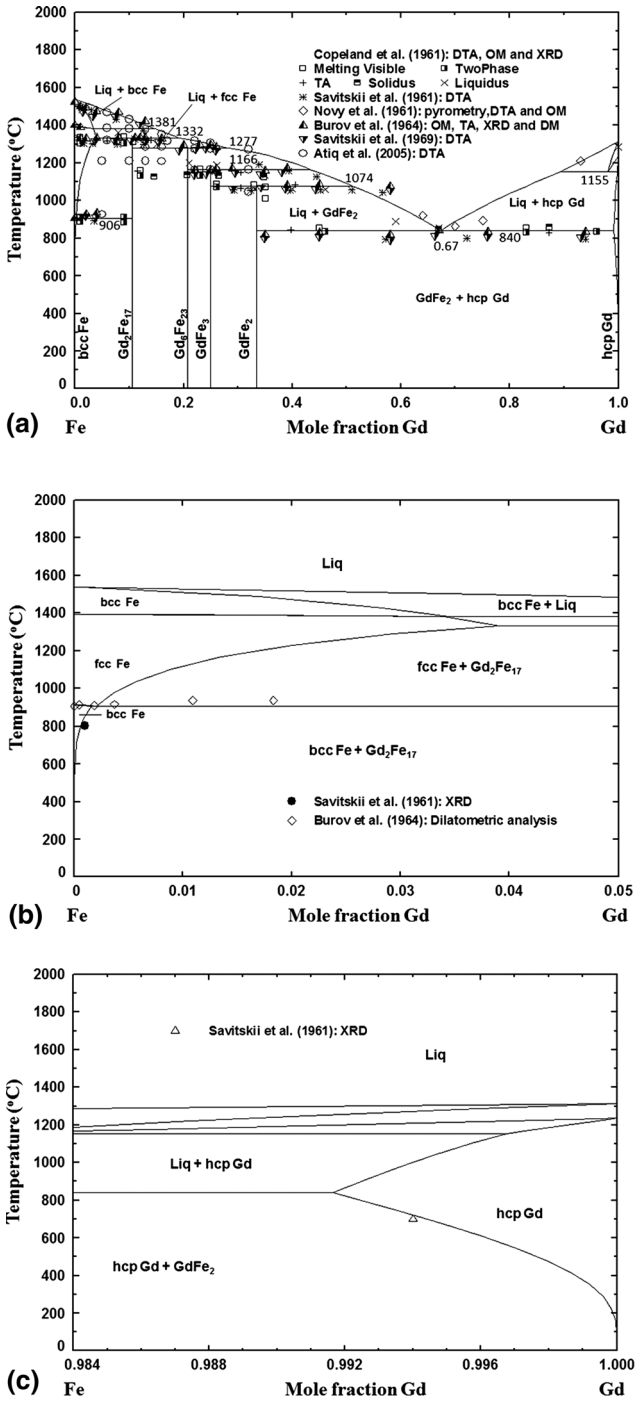

Fig. 1 The optimized phase diagram of the Fe-Gd system with experimental data (a) overall composition range,[44,46–50] (b) in the Fe-rich side,[46,48] and (c) in the Gd-rich side[46]

hcp Gd solution was also needed to reproduce the rapidly increasing solubility of Fe in hcp Gd solution by Savitskii et al.[46]

The integral and the partial enthalpy of mixing of the Fe-Gd liquid were reported by Nikolaenko and Nosova[51] at 1850 K and Ivanov et al.[52] at 1833 K as presented in Fig. 2. The experiments were conducted using a high flux high-temperature isoperibolic calorimeter (SC) under high purity[51] Ar and He[52] gas. Nikolaenko and Nosova[51] used yttria-coated alumina crucibles, whereas in the recent study by Ivanov et al.[52] the partial enthalpy of mixing of the Fe-rich and the Gd-rich compositions was measured using zirconia crucibles and Mo crucibles, respectively. The integral enthalpy of mixing was calculated at 1833 K and presented in Fig. 2(a). Even though the two sets of experimental data show negative enthalpy of mixing, a large discrepancy in terms of the location of minima of enthalpy of mixing and partial enthalpies of Fe and Gd is observed. It is rather unusual to have minima of enthalpy of mixing where no solid compound exists. In addition, the results of Ivanov et al.[52] are consistent with the systematic trend of enthalpy of mixing of all other binary liquid Fe-RE solutions, which will be discussed later in section 4. Therefore, the present model parameters of liquid solution were optimized to reproduce the more recent enthalpy data by Ivanov et al.[52] in Fig. 2 and the phase diagram in Fig. 1, simultaneously.

The ΔH^o_{298} of $GdFe_2$, $GdFe_3$, and Gd_2Fe_{17} were measured by Colinet et al.[53,54] and of $GdFe_2$ by Meschel et al.,[55] as presented in Fig. 3. Colinet et al.[53,54] prepared samples with Gd (99.9 wt.%) and Fe (99.99 wt.%) and conducted experiments by solution calorimetry in molten Al (SC-Al) at about 1000 K and reported the ΔH^o_{298} for $GdFe_2$, $GdFe_3$, and Gd_2Fe_{17} to be −11.6, −9.3 and −2.3 kJ mol-atom^{-1}, respectively. Meschel et al.[55] performed direct synthesis calorimetry (DSCa) of $GdFe_2$ at 1100 °C (1373 K) which contained up to 5 wt.% Gd_2Fe_{17} as an impurity. But it should be noted that the melting of $GdFe_2$ occurs at 1074 °C (1347 K) according to the phase diagram in Fig. 1, and therefore the measurement of Meschel et al.[55] is less reliable. Deodhar and Ficalora[56] also reported the ΔH^o_{298} of the $GdFe_2$ compound from their DTA experiments. The reported values were not reliable due to several kinetic limitations of the formation reaction, along with reported complex reaction mechanisms and C_p assumptions.

Figure 4 shows the C_p of the $GdFe_2$ compound measured by Germano et al.[57] using adiabatic calorimetry (AC) from 15 to 300 K. In the present study, high-temperature C_p was firstly obtained using N–K rule and then modified to fit the low-temperature C_p data by increasing the temperature independent C_p term by 12.31 J mol^{-1}-K^{-1}. The magnetic properties (Bohr magnetons per mole and Curie temperature) of the intermetallic phases were incorporated into the present modeling from Segal and Wallace.[58] As there are no heat capacity data reported for other compounds, the C_p of $GdFe_3$, Gd_6Fe_{23} and Gd_2Fe_{17} were estimated from the N–K rule using the C_p function of

Table 3 Calculated invariant reactions in the Fe-Gd system along with the experimental data

Type	Reaction	Composition (X_{Gd} in liquid)	T, °C	References
Metatectic	bcc Fe → Liq + fcc Fe	0.147	1381	This work
		0.161(a)	1360	45
		0.094(a) ± 0.007	1388 ± 15	44
		0.159(a)	1380 ± 10	46
		0.137(a)	1389 ± 5	49
		0.087(a)	1380	39[A]
		0.092(a)	1381	40[A]
Peritectic	Liq + fcc Fe → Gd_2Fe_{17}	0.191	1332	This work
		0.193(a)	1335 ± 10	45
		0.133(a) ± 0.007	1320 ± 15	44
		0.182(a)	1325	49
		0.119	1328	39[A]
		0.121(a)	1337	40[A]
Peritectic	Liq + Gd_2Fe_{17} → Gd_6Fe_{23}	0.281	1277	This work
		0.283(a)	1282	49
		0.235(a)	1274	39[A]
		0.210(a)	1284	40[A]
Peritectic	Liq + Gd_6Fe_{23} → $GdFe_3$	0.432	1166	This work
		0.408(a)	1160 ± 10	46
		0.433(a)	1171	49
		0.478(a)	1156	39[A]
		0.469(a)	1163	40[A]
Peritectic	Liq + $GdFe_3$ → $GdFe_2$	0.510	1074	This work
	Liq + Gd_2Fe_{17} → $GdFe_2$	0.557	1080 ± 10	45
		0.580(a)	1050	50
		0.403(a) ± 0.007	1080 ± 15	44
		0.592(a)	1080 ± 10	46
		0.584(a)	1057	49
		0.561(a)	1082	39[A]
		0.560(a)	1083	40[A]
Eutectic	Liq → $GdFe_2$ + hcp Gd	0.673	840	This work
		0.723	830 ± 7	45
	Liq → Gd_2Fe_3(b) + hcp Gd	0.704(a)	860	50
		0.670(a) ± 0.007	845 ± 15	44
		0.716(a)	830 ± 7	46
		0.734(a)	829	39[A]
		0.710(a)	832	40[A]
Metatectic	bcc Gd → Liq + hcp Gd	0.896	1155	This work

(a) Extracted from the original phase diagram. (b) The original compounds had different stoichoiometry which was later changed. A: Assessment, Liq: liquid

$GdFe_2$ and Fe, and the magnetic properties were taken into account. The S^o_{298} of $GdFe_2$ derived from the above low-temperature C_p data is 115.6 J mol^{-1} K^{-1}. It should also be noted that Meschel et al.[55] measured the heat content change ($H_{1373} - H_{298}$) of $GdFe_2$ to be 50.8 ± 1.3 kJ mol-atom^{-1}. The calculated value of 40.04 kJ mol-atom^{-1} from the optimized heat capacity in Fig. 4 is quite different from the data of Meschel et al.[55]

Although the phase diagram of the Fe-Gd system is reasonably well determined, the experimental thermodynamic properties of solid phases are insufficient to constrain the Gibbs energies. Based on the phase diagram data, liquid enthalpy data, and limited thermodynamic data of solid compounds, the model parameters of all phases were optimized. Five parameters including two small temperature dependent terms were required to

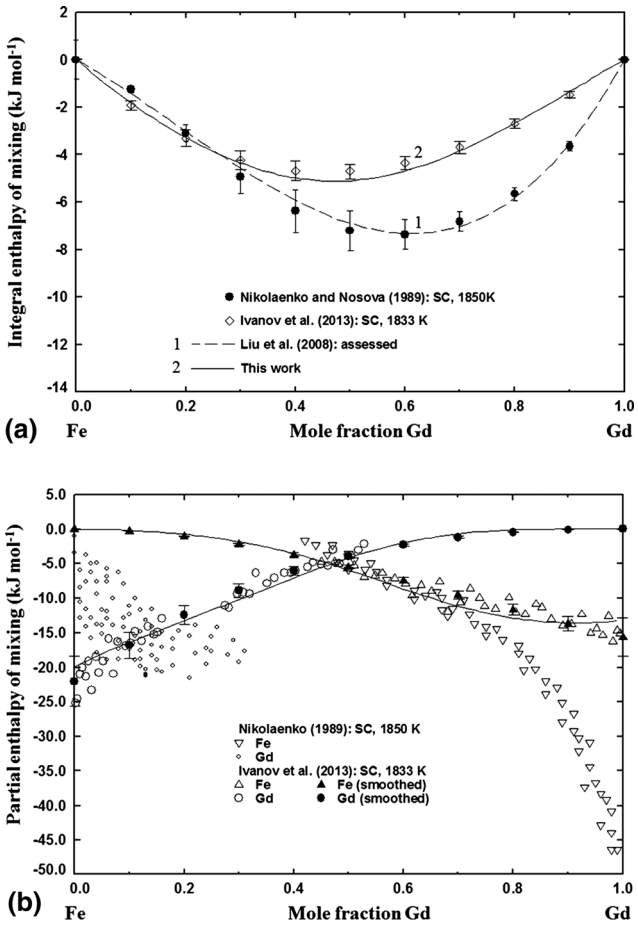

Fig. 2 Enthalpy of mixing of the Fe-Gd liquid at 1850 K with the experimental data[51,52] and assessment.[39] (a) Integral enthalpy of mixing and (b) partial enthalpy of mixing

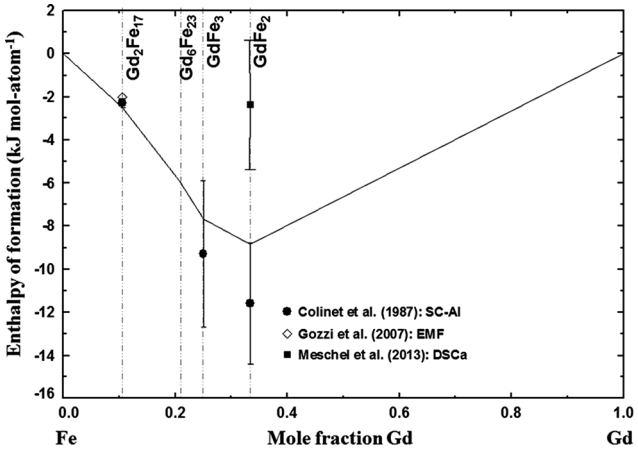

Fig. 3 Enthalpy of formation at 298 K (ΔH^{o}_{298}) of the intermetallic Fe-Gd compounds compared with the experimental data[53,54]

describe the Gibbs energy of liquid phase. The enthalpies of formation of solid compounds by Colinet et al.[53,54] were mostly well reproduced within the experimental error limits. However, it was very difficult to exactly

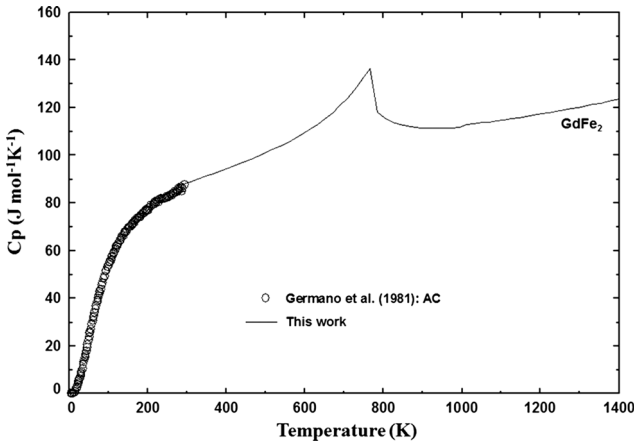

Fig. 4 The optimized C_p of $GdFe_2$ along with the experimental data[57]

reproduce the S^{o}_{298} of $GdFe_2$, 115.6 J mol^{-1} K^{-1} as derived from low-temperature C_p data. The optimized value from the present study is 109.38 J mol^{-1} K^{-1}, which is well constrained by the experimental data of ΔH^{o}_{298} and C_p of $GdFe_2$ and the thermodynamic properties of the liquid phase in conjunction with the phase diagram. All model parameters obtained from the present study are summarized in Table 2.

In all the previous assessments by Liu et al.,[39] Zinkevich et al.[40] and Konar,[41] the liquid enthalpy was optimized using the data by Nikolaenko and Nosova[51] as the experiments of Ivanov et al.[52] were not available at the time of the assessments. Liu et al.[39] assessed the ΔH^{o}_{298} for Gd_2Fe_{17}, $GdFe_3$, and $GdFe_2$ to be −3.74, −8.29 and −9.47 kJ mol-atom^{-1}, respectively, which are consistent with the results of Colinet et al.[53,54] However, Gibbs energy of eight compounds (Gd_2Fe_{17}, Gd_6Fe_{23}, $GdFe_3$, $GdFe_2$, $GdFe_5$, Gd_2Fe_7, Gd_3Fe and Gd_4Fe_3) were defined. Moreover, the S^{o}_{298} of $GdFe_2$ was determined to be 143.86 J mol^{-1} K^{-1} which is much higher than the experimental data of 115.6 J mol^{-1} K^{-1}.[57] The phase equilibria below 900 K were not shown. In the assessment by Zinkevich et al.,[40] the ΔH^{o}_{298} of Gd_2Fe_{17}, $GdFe_3$, and $GdFe_2$, were −3.66, −4.91 and −4.59 kJ mol-atom^{-1}, respectively, which significantly deviate from the results of Colinet et al.[53,54] The C_p of $GdFe_2$ by Germano et al.[57] was not considered, and the S^{o}_{298} for $GdFe_2$ was modeled to be 128.5 J mol^{-1} K^{-1} deviating from experimental 115.6 J mol^{-1} K^{-1}.[57] In addition, their liquid Gibbs energy function was modeled with several large temperature-dependent parameters. In both the assessments by Liu et al.[39] and Zinkevich et al.,[40] all the ΔH^{o}_{298} and S^{o}_{298} of intermetallic compounds were not concomitantly optimized, and therefore several intermetallic phases were calculated to be unstable at room temperature.

3.2 The Fe-Tb (Iron-Terbium) System

The Fe-Tb system was reviewed by Okamoto[59] and assessed by Landin and Ågren[60] and Konar.[41] Landin and Ågren[60] and Konar[41] suggested four stable intermetallic phases Tb_2Fe_{17}, Tb_6Fe_{23}, $TbFe_3$, and $TbFe_2$, which is characteristic of the Fe-heavy RE systems, in addition to bcc Fe, fcc Fe, hcp Tb, bcc Tb solution and liquid phase, based on the experimental study of Dariel et al.[61]

The phase diagram of the Fe-Tb system is shown in Fig. 5 along with experimental data by Dariel et al.,[61] Orlova et al.[62] and Chen et al.[63] Dariel et al.[61] used both TA and quenching experiments followed by XRD, OM, and electron probe microanalysis (EPMA) for phase analysis. Orlova et al.[62] determined the melting point of the compounds by a pyrometer with an error of ± 50 °C followed by compositional chemical analysis. Overall results of Orlova et al.[62] are not reliable as shown in Fig. 5. Dariel et al.[61] reported that Tb_2Fe_{17}, $TbFe_3$, and $TbFe_2$ formed peritectically at 1312, 1212, and 1187 °C, respectively, and also reported the eutectic reaction Liq → $TbFe_2$ + hcp Tb at 847 °C. Recently, Chen et al.[63] re-examined the phase diagram in the composition range of 0.045 to 0.1625 mol fraction Tb carefully using DTA (see Fig. 5(b)). The DTA results for Tb_2Fe_{17} compound show a congruent melting at 1316 °C and a eutectic reaction of Liq → Tb_2Fe_{17} + bcc Fe at 1301 °C with 0.075 mol fraction Tb. While Dariel et al.[61] reported two polymorphic forms of Tb_2Fe_{17} (α-Tb_2Fe_{17} with Th_2Zn_{17}-type rhombohedral in Tb-rich side and β-Tb_2Fe_{17} with Th_2Ni_{17}-type hexagonal in Fe-rich side), Chen et al.[63] reported the presence of only one polymorph of Tb_2Fe_{17} (Th_2Ni_{17} structure) from DTA study. According to Chen et al.,[63] Tb_2Fe_{17} was observed at the solidification temperature with no homogeneity range. As part of the phase diagram study of the Fe-Pt-Tb system, Gu et al.[64] also confirmed the existence of a stoichiometric Tb_2Fe_{17} with Th_2Zn_{17} type rhombohedral structure at 900 °C (1173 K) with XRD. In the present study, a single stoichiometric phase of Tb_2Fe_{17} was considered without polymorphic transition. Dariel et al.[61] reported limited solid solution of Tb in bcc Fe at 880 °C to be 0.0007 ± 0.0003 and 0.001 ± 0.0005 mol fraction of Tb by XRD lattice parameter measurements and EPMA analysis, respectively. No measurable solubility of Tb in fcc Fe was observed by Dariel et al.[61] The solubility of Tb in bcc Fe is depicted in Fig. 5(c). Overall, the phase diagram study by Dariel et al.[61] is reliable except the melting behavior of Tb_2Fe_{17} which was further properly examined by Chen et al.[63]

Figure 6(a) and (b) show the integral and partial enthalpies of mixing of liquid Fe and Tb measured by Ivanov et al.[52] using a SC at 1833 K. Ivanov et al.[52] measured the partial enthalpy of mixing of the Fe-rich alloys using zirconia crucible and Tb-rich compositions using molybdenum

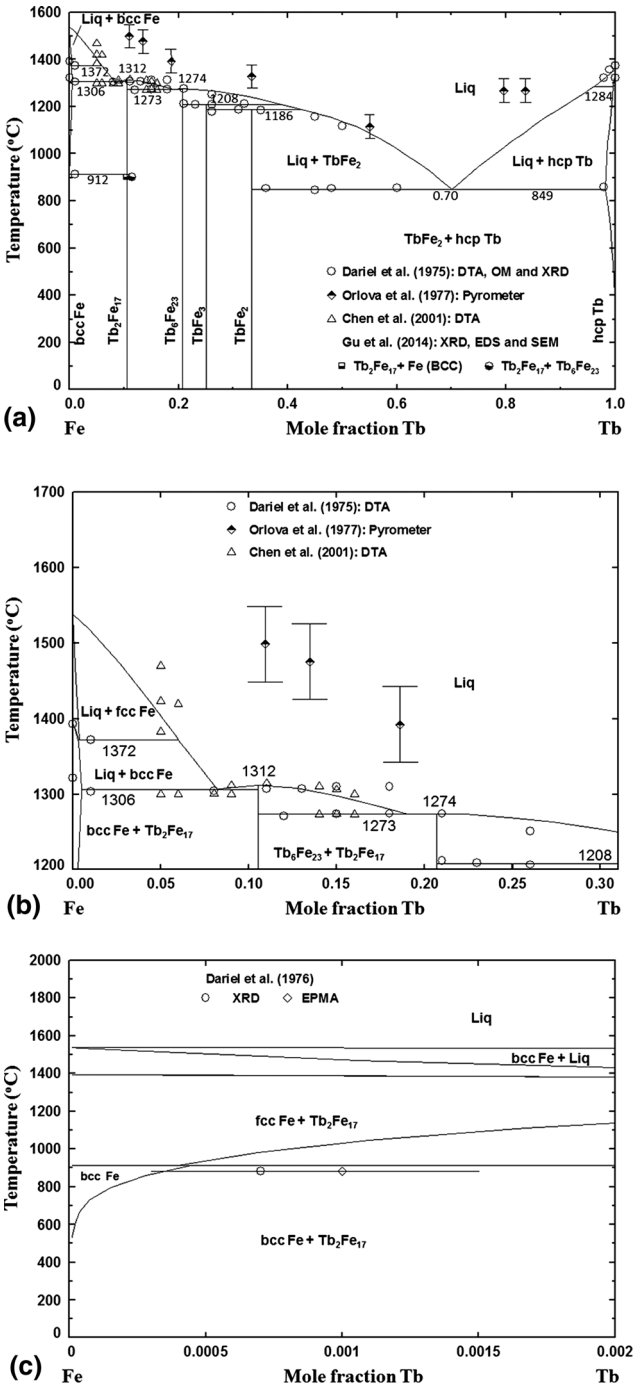

Fig. 5 The optimized phase diagram of the Fe-Tb system with the experimental data (a) overall composition range,[61–64] (b) in the high-temperature region[61–63] (c) in the Fe-rich side[61]

crucible. A smoothed equation for integral enthalpy of mixing was obtained with a minimum at 0.45 mol fraction Tb with a value of −5.06 ± 0.43 kJ mol^{-1}. The present optimization reproduced these experimental data accurately. At the time of previous assessments by Landin and Ågren,[60] and Konar,[41] no such experimental enthalpy of mixing data were available, hence the estimated enthalpies

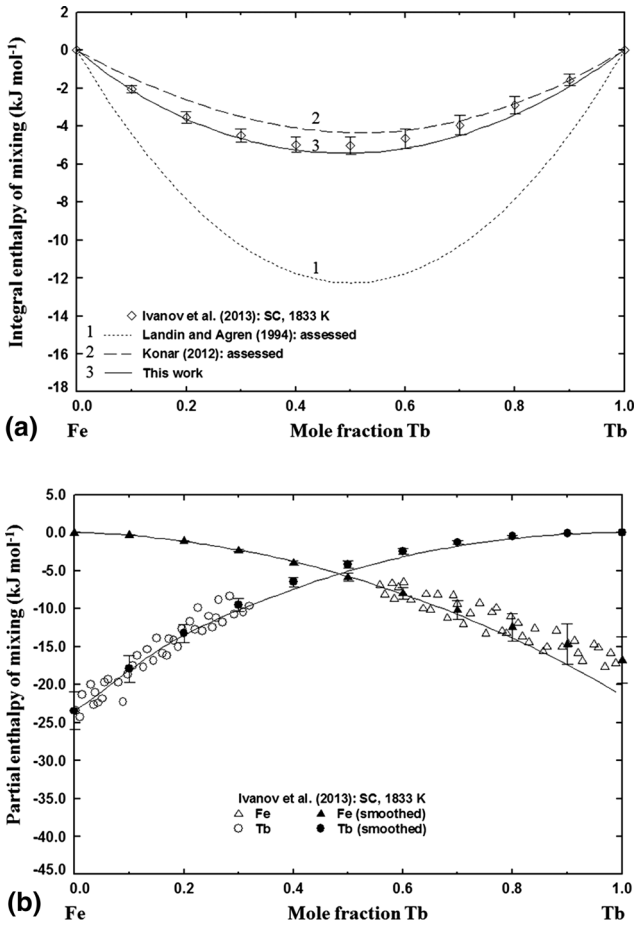

Fig. 6 Enthalpy of mixing of the Fe-Tb liquid at 1833 K with the experimental data[52] and assessments.[41,60] (a) Integral enthalpy of mixing and (b) partial enthalpy of mixing

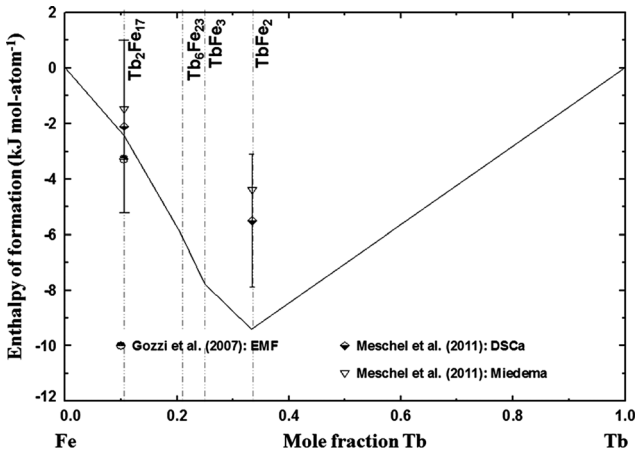

Fig. 7 Enthalpy of formation at 298 K (ΔH^{o}_{298}) of the intermetallic Fe-Tb compounds compared with the experimental data[55,65]

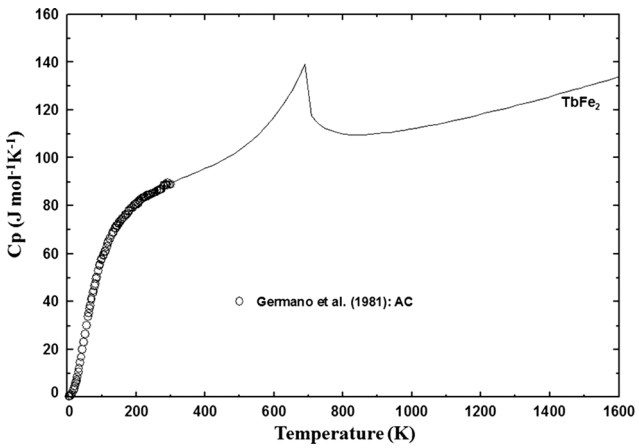

Fig. 8 The optimized C_p of $TbFe_2$ along with the experimental data[57]

are quite different from the present result as shown in Fig. 6(a).

The ΔH^{o}_{298} of Tb_2Fe_{17} and $TbFe_2$ measured by Gozzi et al.[65] and Meschel et al.[55] are presented in Fig. 7. Gozzi et al.[65] reported the ΔH^{o}_{298} for the Tb_2Fe_{17} phase derived from the Gibbs energy of formation determined using galvanic cells with CaF_2 electrolyte. Meschel et al.[55] determined the formation enthalpies of Tb_2Fe_{17} and $TbFe_2$ by DSCa, and also reported the predicted values from Miedema method. The experimental data and estimated data from Miedema method are consistent within the experimental error limits. The experimental value of ΔH^{o}_{298} for Tb_2Fe_{17} was measured to be -2.1 ± 3.1 and -3.3 kJ mol-atom^{-1} by Meschel et al.[55] and Gozzi et al.,[65] respectively, which is reproduced as -2.45 kJ mol-atom^{-1} in the present optimization. The experimental ΔH^{o}_{298} value of $TbFe_2$ by Meschel et al. was -5.5 ± 2.4 kJ mol-atom^{-1} and the present optimized value is about 1.5 kJ mol-atom^{-1} more negative than the experimental error range of their data.

Figure 8 shows the experimental low-temperature C_p of $TbFe_2$ measured by Germano et al.[57] using AC from 4.2 K to 300 K and the C_p curve from the present study. The S^{o}_{298} of $TbFe_2$ was determined to be 122.7 J mol^{-1} K^{-1}, from the experimental low-temperature C_p. The estimated high-temperature C_p of $TbFe_2$ presented in Fig. 8 was firstly derived using the N–K rule and the temperature independent term of C_p was modified by 9.09 J mol-K to fit the low-temperature C_p data. The magnetic moment and the Curie temperature of the compounds were obtained from Buschow.[66] The C_p of the other compounds $TbFe_3$, Tb_6Fe_{23}, and Tb_2Fe_{17} were also estimated by the N–K rule from the C_p of hcp Tb and bcc Fe, and the magnetic properties reported by Buschow[66] were taken into account.

The present optimization of the Fe-Tb system was carried out by following a similar procedure like the Fe-Gd system. The enthalpy of the liquid phase and the Gibbs energy of $TbFe_2$ were firstly optimized together with the phase diagram information in order to reproduce the

enthalpy of mixing by Ivanov et al.[52] and the thermodynamic properties of $TbFe_2$ compound. Then, the thermodynamic properties of ΔH^{o}_{298} and S^{o}_{298} of $TbFe_3$, Tb_6Fe_{23} and Tb_2Fe_{17} and the bcc solution parameters were optimized to reproduce their phase stabilities. Six model parameters including temperature-dependent terms were required to describe the Gibbs energy of liquid phase. The regular solution parameter with temperature dependent term was determined to reproduce the solubility of Tb in bcc Fe. The parameters for fcc and hcp solutions were determined to reproduce the associated invariant reaction temperatures. In the literature, no experimental homogeneity range data for these solutions are available. In general, the phase diagram data and the enthalpy of formation data by Meschel et al.[55] were well reproduced. The optimized S^{o}_{298} of $TbFe_2$ (116.8 J mol^{-1} K^{-1}) is slightly smaller than the experimentally determined value (122.7 J mol^{-1} K^{-1}). In the present study, the congruent melting of Tb_2Fe_{17} at 1312 °C is calculated which is consistent with the detailed experimental study by Chen et al.[63] (1316 °C), while Dariel et al.[61] proposed a peritectic melting of this compound. It should be also noted that the congruent melting of the RE_2Fe_{17} compound was observed in the Fe-Dy, and Fe-Ho system (see next sections). Although Dariel et al.[61] reported the incongruent melting of the Tb_6Fe_{23} at 1276 °C, it is optimized to be congruent melting at 1274 °C in the present study. According to the liquidus of Tb_2Fe_{17} by Chen et al.[63] (see Fig. 6(b)), it is very difficult to get the incongruent melting of Tb_6Fe_{23}. So, the present study is more consistent with the experimental results by Chen et al. All other invariant reactions in the Fe-Tb system are in good agreement with experimental data, as summarized in Table 4.

3.3 The Fe-Dy (Iron-Dysprosium) System

The Fe-Dy system was reviewed by Okamoto[67] and thermodynamically assessed by Landin and Ågren[60] and Konar et al.[68] Four intermetallic phases, $DyFe_2$, $DyFe_3$, Dy_6Fe_{23}, and Dy_2Fe_{17} were considered as stable intermetallic compounds. In the present study, the previous model parameters of Konar et al.[68] were slightly modified to reproduce new experimental data by Nagai et al.[69] for activity and Ivanov et al.[52] for liquid enthalpy.

The optimized phase diagram of the Fe-Dy system is shown in Fig. 9 along with the experimental data of Van der Goot and Buschow.[70] Van der Goot and Buschow investigated the phase diagram over the whole composition

Table 4 Calculated invariant reactions in the Fe-Tb system along with the experimental data

Type	Reaction	Composition (X_{Tb} in liquid)	T, °C	References
Metatectic	bcc Fe → Liq + fcc Fe	0.059	1372	This work
Eutectic	Liq + fcc Fe → Tb_2Fe_{17}	0.082	1306	This work
		0.075	1301	63
Congruent	Liq → Tb_2Fe_{17}	0.105	1312	This work
			1316	63
Eutectic	Liq → Tb_2Fe_{17} + Tb_6Fe_{23}	0.190	1273	This work
Peritectic(b)	Liq + fcc Fe → Tb_2Fe_{17}	0.173	1312 ± 3	61
		0.118	1317	60[A]
Congruent	Liq → Tb_6Fe_{23}	0.207	1274	This work
Peritectic(b)	Liq + Tb_2Fe_{17} → Tb_6Fe_{23}	0.212(a)	1276 ± 3	61
		0.204(a)	1276	60[A]
Peritectic	Liq + Tb_6Fe_{23} → $TbFe_3$	0.388	1208	This work
		0.346(a)	1212 ± 3	61
		0.349(a)	1214	60[A]
Peritectic	Liq + $TbFe_3$ → $TbFe_2$	0.424	1186	This work
		0.410(a)	1187 ± 3	61
		0.394(a)	1187	60[A]
Eutectic	Liq → $TbFe_2$ + hcp Tb	0.700	849	This work
		0.720 ± 0.005	847 ± 3	61
		0.716(a)	839	60[A]
Metatectic	bcc Tb → Liq + hcp Tb	0.962	1284	This work
		0.970	1318 ± 2	61
		0.970(a)	1290	60[A]

(a) Extracted from the original phase diagram. (b) The previous authors assumed peritectic meltings of Tb_2Fe_{17} and Tb_6Fe_{23} instead of the congruent melting. A: Assessment

range of the Fe-Dy system by means of TA and quenching experiment with OM and XRD phase analysis. Based on the experimental micrographs, they suggested that $DyFe_3$ and Dy_2Fe_{17} melted congruently while Dy_6Fe_{23} and $DyFe_2$ melted peritectically. The mutual solubilities of Fe and Dy have not been studied, but the transition temperature of bcc and fcc Fe phase indicates the very small amount of the solubility of Dy in Fe if it exists.

Figure 10 shows the integral and partial enthalpies of mixing of the Fe-Dy liquid phase measured by Ivanov et al.[52] using a SC. Ivanov et al.[52] measured the partial enthalpy of mixing of Fe-rich alloys using zirconia crucible and Dy-rich compositions using molybdenum crucible at 1833 K. A smoothed equation for integral enthalpy of mixing was obtained with a minimum at 0.35 mol fraction Dy with a value of -8.80 ± 1.33 kJ mol^{-1}. The previous assessment results from Konar et al.[68] are slightly higher than experimental data of Ivanov et al.[52]

In Fig. 11, the ΔH^o_{298} determined by the present assessment is depicted along with experimental data reported by Norgren et al.,[71] Gozzi et al.[65] and Meschel et al.[55] The ΔH^o_{298} of $DyFe_2$, $DyFe_3$ and Dy_2Fe_{17} were measured by Norgren et al.[71] using SC-Al at 1100 K. The reported ΔH^o_{298} of compounds become more negative with increasing Dy content. Gozzi et al.[65] and Meschel et al.[55] reported ΔH^o_{298} of Dy_2Fe_{17} and $DyFe_2$ from EMF measurements and DSCa, respectively, and also conducted empirical Miedema calculations, as shown in Fig. 11. The experimental ΔH^o_{298} value of Meschel et al.[55] of $DyFe_2$ is more positive than the value of Dy_2Fe_{17}, which is a completely opposite trend from Norgren et al.[71] As seen in all Fe-RE system, the optimized ΔH^o_{298} of compounds become more negative with increasing RE content. Therefore, the result of Norgren et al.[71] was considered more accurate in the present optimization.

The low-temperature C_p of $DyFe_2$ was measured by Germano et al.[57] using an AC as presented in Fig. 12. Germano et al. calculated the S^o_{298} of $DyFe_2$ from the heat

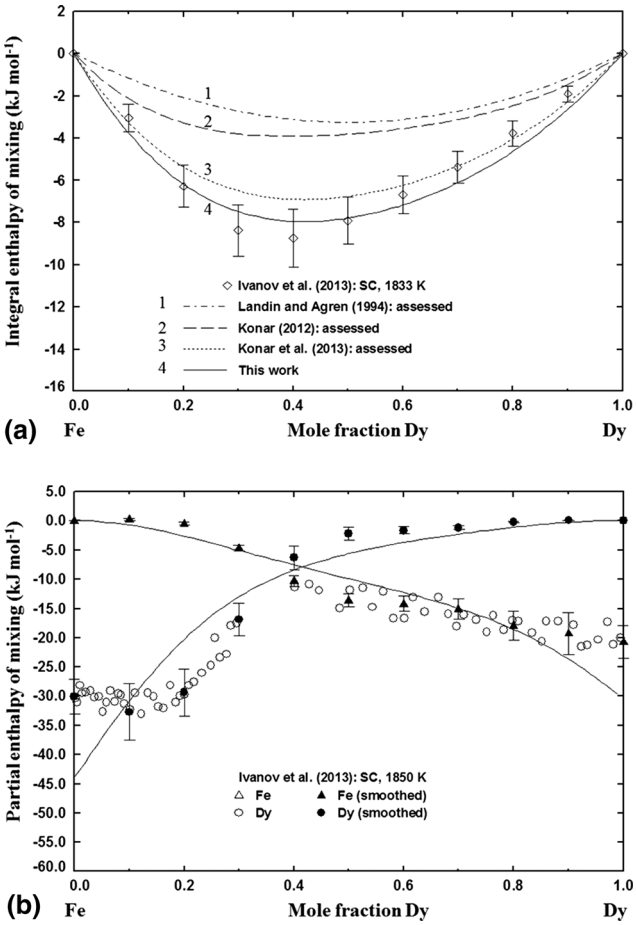

Fig. 10 Enthalpy of mixing of the Fe-Dy liquid at 1850 K with the experimental data[52] and assessments[68] (a) Integral enthalpy of mixing and (b) partial enthalpy of mixing

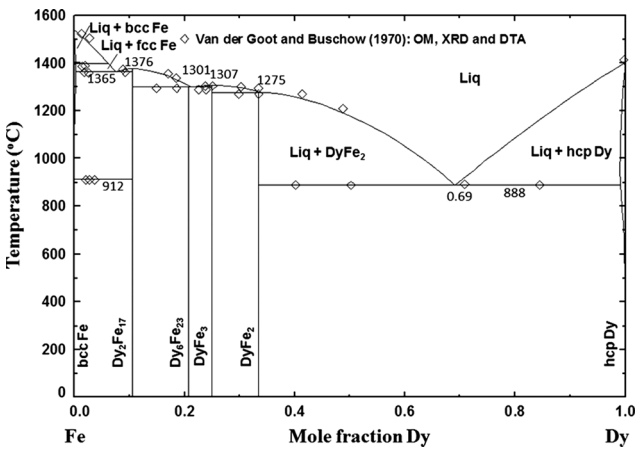

Fig. 9 The optimized phase diagram of the Fe-Dy system with the experimental data[70]

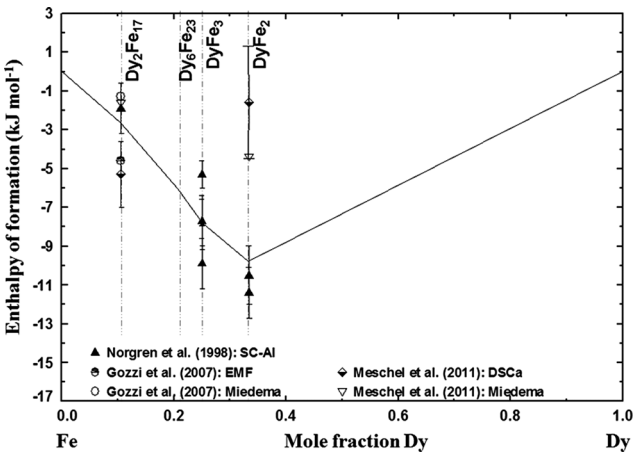

Fig. 11 Enthalpy of formation at 298 K (ΔH^o_{298}) of the intermetallic Fe-Dy compounds compared with the experimental data[55,65,71]

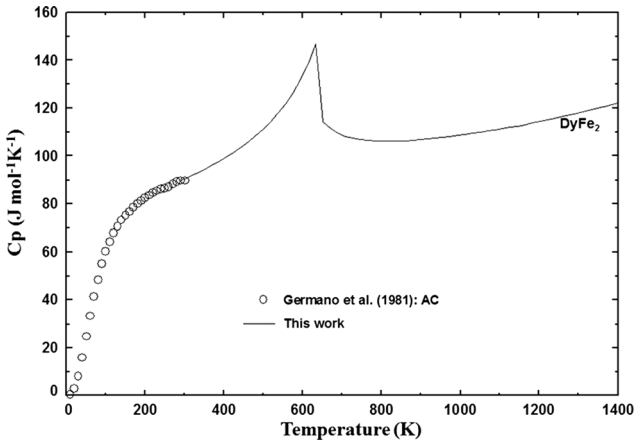

Fig. 12 The optimized C_p of $DyFe_2$ along with the experimental data[57]

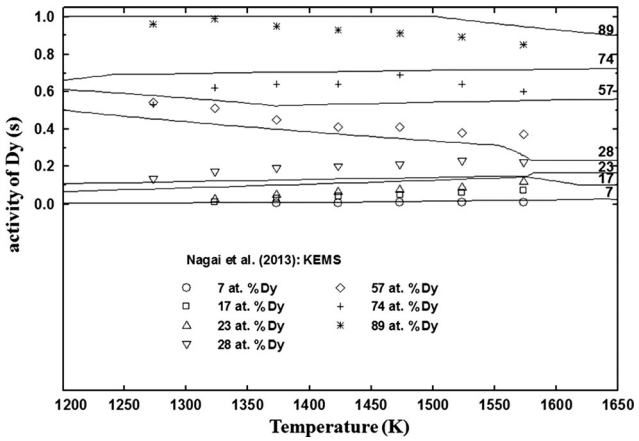

Fig. 13 The temperature dependence of the activity of Dy of 7, 17, 23, 28, 57, 74 and 89 at.% Dy Fe-Dy alloys with the experimental data[69]

capacity data to be 124.8 J mol^{-1} K^{-1}. Like the previous systems, the high-temperature C_p for $DyFe_2$ phase was formulated based on the N–K rule with small adjustment as tabulated in Table 2. As there are no data available, the C_p of $DyFe_3$, Dy_6Fe_{23} and Dy_2Fe_{17} was estimated using the N–K rule. The magnetic contributions to the C_p of all intermetallic compounds were taken into account using the compilation data by Buschow.[66]

Nagai et al.[69] measured the thermodynamic properties of several compositions in the temperature range of 1273 to 1573 K using the Knudsen effusion mass spectrometry (KEMS). Several alloys were prepared at 0.07, 0.17, 0.23, 0.28, 0.57, 0.74, and 0.89 mol fraction of Dy using electron beam melting technique with reagent grade Dy and electrolytic Fe. The chemical compositions of the alloys are verified by inductively coupled plasma atomic emission spectroscopy (ICP-AES) and phases were identified by XRD before KEMS experiment. The ion currents were detected for Dy with the isotopes, ^{158}Dy, ^{160}Dy, ^{161}Dy, ^{162}Dy, ^{163}Dy, and ^{164}Dy. However, the ion currents due to ^{54}Fe, ^{56}Fe, ^{57}Fe and ^{58}Fe isotopes were not detected, as the vapor pressures in equilibrium with the alloys were assumed to be low. The activities of Dy of different alloys derived from KEMS measurement are summarized in Fig. 13.

In the present optimization, all the available experimental data of thermodynamic properties and phase diagram was simultaneously considered. The enthalpy of mixing data for the liquid phase is well reproduced in Fig. 10. The Gibbs energy of $DyFe_2$ can be relatively well defined from ΔH^o_{298}, S^o_{298} and C_p data in Fig. 11 and 12. The optimized ΔH^o_{298} is in good agreement with the experimental data by Norgren et al.,[71] and S^o_{298} of $DyFe_2$ was optimized to be 118.10 J mol^{-1} K^{-1} which is slightly lower than the value 124.8 J mol^{-1} K^{-1} derived from low-temperature heat capacity data by Germano et al.[57] The ΔH^o_{298} and S^o_{298} of $DyFe_3$, Dy_6Fe_{23} and Dy_2Fe_{17} were optimized to reproduce their melting point and the phase diagram. All invariant reactions of the Fe-Dy system are summarized in Table 5. In general, the calculated invariant reactions are consistent with experimental data by Van der Goot and Buschow[70] within ± 10 °C, except the invariant reactions related to Dy_6Fe_{23}; the largest difference is calculated for the eutectic reaction Liq → Dy_6Fe_{23} + $DyFe_3$ which is calculated to be 15 °C higher than the experimental data. The optimized activity data of Dy in Fig. 13 is in reasonable agreement with the measured data by Nagai et al.[69] In fact, the activity data of Dy in the alloy up to 0.28 mol fraction of Dy below 1573 K are directly determined from the Gibbs energies of intermetallic phases, and the calculated values are in reasonable agreement with the experimental data, which proves that the optimized thermodynamic properties of solid compounds are reasonable. Considering the difficulty in obtaining accurate Dy activity as pointed out by Nagai et al.[69] themselves, more weight was put on the phase diagram data in the present optimization. It should be mentioned that similar incoherencies of the data by Nagai et al.[72] were also pointed out in our previous assessment for the Fe-La system.[31]

The Fe-Dy system was thermodynamically assessed by Landin and Ågren,[60] Konar[41] and Konar et al.[68] In the assessment done by Landin and Ågren,[60] the ΔH^o_{298} of the compounds were not constrained by the experimental data of Norgren et al.[71] Moreover, their optimization was viable only above 527 °C (800 K), and the magnetic contributions to the Gibbs energies of the compounds were not considered. Landin and Ågren[60] also calculated the formation of Dy_6Fe_{23} by a peritectoid reaction rather than an experimental peritectic reaction.[70] In the all previous thermodynamic assessments, the integral enthalpy of

Table 5 Calculated invariant reactions in the Fe-Dy system along with the experimental data

Type	Reaction	Composition (X_{Dy} in liquid)	T, °C	References
Eutectic	Liq → fcc Fe + Dy_2Fe_{17}	0.074	1365	This work
		0.091(a)	1360	70
		0.081(a)	1368	60[A]
Congruent	Liq → Dy_2Fe_{17}	0.105	1376	This work
			1375	70
			1368	60[A]
Peritectic	Liq + Dy_2Fe_{17} → Dy_6Fe_{23}	0.210	1301	This work
		0.214(a)	1290	70
Peritectoid	$DyFe_3$ + Dy_2Fe_{17} → Dy_6Fe_{23}	…	1281	60[A]
Eutectic	Liq → Dy_6Fe_{23} + $DyFe_3$	0.215	1300	This work
		0.220(a)	1285	70
		0.236(a)	1295	60[A]
Congruent	Liq → $DyFe_3$	0.250	1307	This work
			1305	70
			1297	60[A]
Peritectic	Liq + $DyFe_3$ → $DyFe_2$	0.339	1275	This work
		0.400(a)	1270	70
		0.354(a)	1263	60[A]
Eutectic	Liq → $DyFe_2$ + hcp Dy	0.691	888	This work
		0.712(a)	890	70
		0.735(a)	877	60[A]

(a) Extracted from the original phase diagram. A: Assessment

mixing was calculated to be less negative than the experimental data as shown in Fig. 10(a).

3.4 The Fe-Ho (Iron-Holmium) System

The Fe-Ho system was reviewed by Kubaschewski[42] and Okamoto[73] and assessed by Kardellass et al.[74] and Konar.[41] Four stable intermetallic compounds, $HoFe_2$, $HoFe_3$, Ho_6Fe_{23}, and Ho_2Fe_{17} exist in the Fe-Ho system.

The optimized phase diagram of the Fe-Ho system in the present study is presented in Fig. 14 along with experimental data. The phase diagram was investigated by Roe and O'Keefe[75] up to 0.77 mol fraction Ho. They established the phase diagram by DTA and quenching experiments followed by XRD and metallographic phase analysis. $HoFe_2$ and $HoFe_3$ were reported to melt peritectically and Ho_6Fe_{23} and Ho_2Fe_{17} were reported to melt congruently. The eutectic reaction of Liq → $HoFe_2$ + hcp Ho was reported at 0.63 mol fraction of Ho and 875 °C. The other two eutectic reactions reported by Roe and O'Keefe[75] are Liq → Ho_2Fe_{17} + Ho_6Fe_{23} at 0.178 mol fraction of Ho and 1284 °C, and Liq → fcc Fe + Ho_2Fe_{17} at 0.083 mol fraction of Ho and 1338 °C. In fact, the nature of melting of $HoFe_2$ was very difficult to be determined in the experiment by Roe and O'Keefe[75] due to the close melting temperatures of $HoFe_2$ and $HoFe_3$. Their

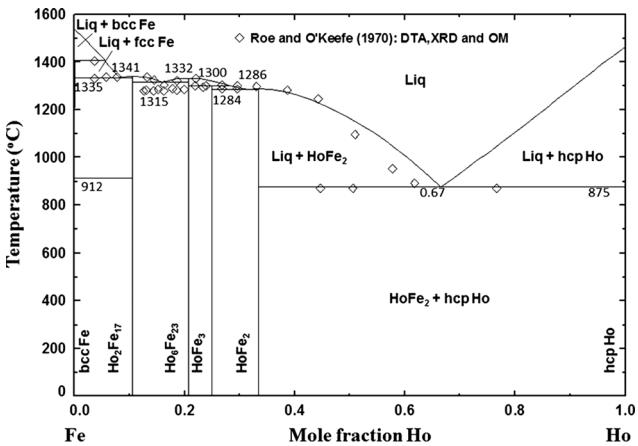

Fig. 14 The optimized phase diagram of the Fe-Ho system with the experimental data[75]

experimental DTA results seem to be more favorable to the congruent melting of $HoFe_2$. In an earlier study by O'Keefe et al.,[76] $HoFe_2$ was reported to melt at 1335 ± 15 °C. Considering the melting temperatures of $HoFe_3$ and Ho_2Fe_{17} in the same study, congruent melting of $HoFe_2$ can be reasonably concluded. However, this result was not taken into account by Roe and O'Keefe[75] later. In the present study, the congruent melting of $HoFe_2$ was assumed considering the melting behavior of $REFe_2$ compound

changing from peritectic (incongruent) to congruent melting with increasing atomic number of RE. For example, $ErFe_2$, $LuFe_2$, and $TmFe_2$ in the succeeding Fe-heavy RE systems melt congruently. The congruent melting behavior of Ho_2Fe_{17} and Ho_6Fe_{23} concur with those in the Fe-Tb and Fe-Dy systems.

Unfortunately, no enthalpy for liquid phase was experimentally determined. In order to constrain the model parameters of liquid phase reasonably, the enthalpy of mixing is necessary. Therefore, in the present study, the enthalpy of mixing of liquid Fe-Ho solution was estimated from the systematic trend in the Fe-RE system. As can be seen in the enthalpy of mixing data through all Fe-RE systems, there is a systematic change in the enthalpy of mixing; with increasing atomic number of RE, it becomes more negative and the location of the minima slowly moves towards the Fe-rich composition. Therefore, the mixing enthalpy of liquid Fe-Ho solution could be estimated to be an average of the experimental mixing enthalpy data of the Fe-Dy (just prior to Ho) and Fe-Er (just next to Ho) solution. Unfortunately, the experimental data of liquid Fe-Er solution is unavailable too. Thus, in the present study, the enthalpy of mixing of liquid Fe-Ho solution was estimated from the Fe-Dy and Fe-Lu solution as $\Delta H_{mix,\text{Fe-Ho}} = \Delta H_{mix,\text{Fe-Dy}} + 0.25\ (\Delta H_{mix,\text{Fe-Lu}} - \Delta H_{mix,\text{Fe-Dy}})$, and the result is shown in Fig. 15. The factor of 0.25 was determined by neglecting Yb (in between Tm and Lu) which does not follow the general periodic trend of the physico-chemical properties of RE elements. Petiffor[77–79] proposed the phenomenological coordinate, called Mendeleev number (M) for each element in the periodic table where M is based on the size, electronegativity, valence and the bond orbitals, and predicts the nature and stoichiometry of compound formation. The M of Yb and Eu are quite different from other RE elements. According to the prediction from Miedema's method, the formation enthalpies of Fe-Yb and Fe-Eu compounds are positive while those of other Fe-heavy RE systems are negative. This means that Yb and Eu are not following the general trend of RE series. Thus, the choice of the present estimation scheme of the enthalpy of mixing of the Fe-Ho liquid solution is in accordance with the results of the Mendeleev number (M) and Miedema's prediction.

The ΔH^o_{298} of Ho_2Fe_{17} and $HoFe_2$ compounds were measured by Gozzi et al.[65] and Meschel et al.,[55] respectively, as shown in Fig. 16. Gozzi et al. derived ΔH^o_{298} of the Ho_2Fe_{17} phase (-6.7 kJ mol-atom^{-1}) from the galvanic cells with CaF_2 electrolyte. Meschel et al. measured the ΔH^o_{298} of $HoFe_2$ using DSCa. The ΔH^o_{298} of $HoFe_2$ is even positive than that of Ho_2Fe_{17}. Moreover, the ΔH^o_{298} values for all the $REFe_2$ compounds by Meschel et al. were found to be systematically more positive than other experimental data and optimized data, and are inconsistent with the minima of the enthalpy of mixing. So the result by Meschel et al. was treated as less reliable.

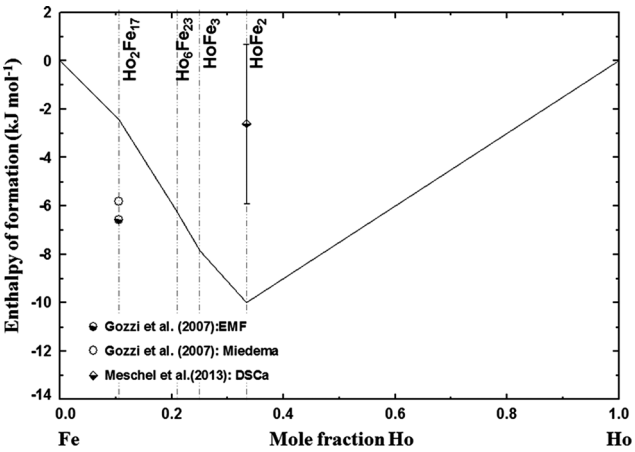

Fig. 16 Enthalpy of formation at 298 K (ΔH^o_{298}) of the intermetallic Fe-Ho compounds compared to the experimental data[55,65]

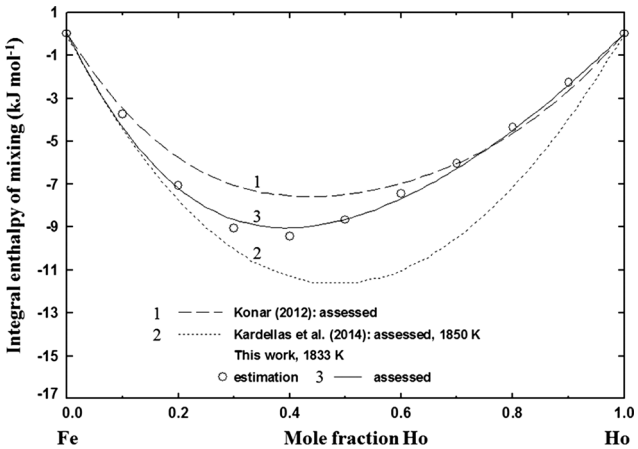

Fig. 15 Integral enthalpy of mixing of the Fe-Ho liquid at 1833 K with assessments[41,74]

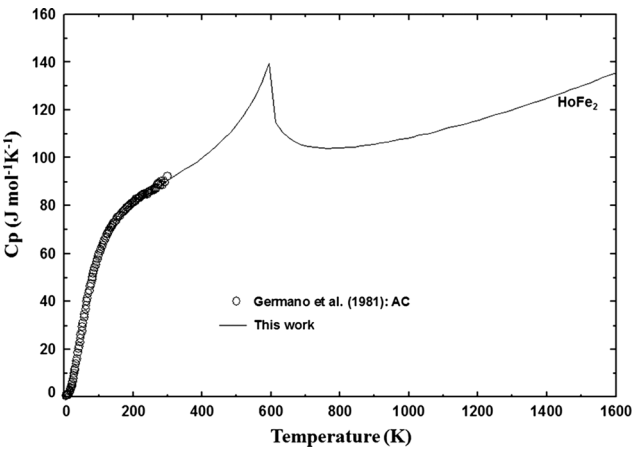

Fig. 17 The optimized C_p of $HoFe_2$ along with the experimental data[57]

Figure 17 shows the low-temperature C_p of $HoFe_2$ measured by Germano et al.[57] using AC. Germano et al.[57] also derived the S^o_{298} (127.4 J mol^{-1} K^{-1}) from the C_p data. The high-temperature C_p for $HoFe_2$ phase was estimated based on the N–K rule with small adjustment as tabulated in Table 2 to reproduce the experimental C_p at 300 K. The heat content ($H_{1373K} - H_{298K}$) of $HoFe_2$ measured by Meschel et al.[55] was 37.4 ± 1.5 kJ mol-atom^{-1} compared to the calculated value 39.56 kJ mol-atom^{-1} in the present study. Thus, the C_p of $HoFe_2$ shown in Fig. 17 is considered to be reliable. The C_p of $HoFe_3$, Ho_6Fe_{23}, and Ho_2Fe_{17} were also estimated from the N–K rule. The magnetic properties (Bohr magnetons and Curie temperatures) of the compounds were obtained from the compilation of Buschow.[66]

Five model parameters including two small temperature dependent terms were determined to describe the thermodynamic behavior of liquid Fe-Ho phase. As mentioned above, the estimated enthalpy of mixing was used to constrain the model parameters of liquid phase first. Then, the thermodynamic data of solid $HoFe_2$ and other compounds were simultaneously considered to optimize the model parameters of all phases in the system to reproduce the phase diagram. The optimized S^o_{298} of $HoFe_2$ is 122.10 J mol^{-1} K^{-1} which is slightly smaller than the experimental data of 127.4 J mol^{-1} K^{-1}.[57] The S^o_{298} of other compounds were slightly adjusted if necessary from those derived from the N–K rule. It should be noted that the congruent melting behavior of $HoFe_2$ was considered instead of peritectic melting as discussed above. All other invariant reactions are well reproduced. The invariant reactions are summarized in Table 6. No measurable mutual solubilities of Fe and Ho in both fcc, bcc and hcp solid solutions were considered in the present optimization.

The previous assessment conducted by Konar[41] has limitation due to the lack of thermodynamic data for the Fe-Ho liquid, similar to the assessment for the Fe-Dy system. In a later optimization by Kardellass et al.,[74] a significantly large temperature dependent term was used to assess the Gibbs energy of the liquid phase of the Fe-Ho system. As shown in Fig. 15, the minimum of the enthalpy of mixing calculated from the study by Kardellass et al. is −11.5 kJ mol^{-1} at 0.5 mol fraction of Ho, which is noticeably different from the estimated data. The assessed ΔH^o_{298} of Ho_2Fe_{17} (−0.295 kJ mol-atom^{-1}) and $HoFe_2$ (−2.65 kJ mol-atom^{-1}) are much smaller than the optimized values in the present study. In fact, their ΔH^o_{298} of $HoFe_2$ is close to that measured by Meschel et al.[55] (−2.6 ± 3.3 kJ mol-atom^{-1}). On the other hand, the S^o_{298} of $HoFe_2$ optimized by Kardellass et al.[74] was

Table 6 Calculated invariant reactions with the experimental data in the Fe-Ho system

Type	Reaction	Composition (X_{Ho} in liquid)	T, °C	References
Eutectic	Liq → fcc Fe + Ho_2Fe_{17}	0.082	1335	This work
		0.083	1338	75
		0.096	1340	74[A]
Congruent	Liq → Ho_2Fe_{17}	0.105	1341	This work
			1343 ± 3	75
			1340	74[A]
Eutectic	Liq → Ho_2Fe_{17} + Ho_6Fe_{23}	0.160	1315	This work
		0.178	1284	75
		0.163	1318	74[A]
Congruent	Liq → Ho_6Fe_{23}	0.207	1332	This work
			1332 ± 3	75
			1330	74[A]
Peritectic	Liq + Ho_6Fe_{23} → $HoFe_3$	0.281	1300	This work
		0.284(a)	1293 ± 3	75
		0.289	1296	74[A]
Congruent	Liq → $HoFe_2$	0.333	1286	This work
			1282	74[A]
Eutectic	Liq → $HoFe_3$ + $HoFe_2$	0.314	1284	This work
Peritectic(b)	Liq + $HoFe_3$ → $HoFe_2$	0.354(a)	1288 ± 3	75
Eutectic	Liq → $HoFe_2$ + hcp Ho	0.665	875	This work
		0.631	875	75
		0.632	873	74[A]

(a) Extracted from the original phase diagram. (b) The previous author assumed peritectic melting of $HoFe_2$ instead of the congruent melting. A: Assessment

149.54 J mol^{-1} K^{-1} which is significantly larger than the experimental data of 127.4 J mol^{-1} K^{-1}.[57]

3.5 The Fe-Er (Iron-Erbium) System

The Fe-Er system was assessed by Konar[41] and Zhou et al.[80] where four stable compounds $ErFe_2$, $ErFe_3$, Er_6Fe_{23}, and Er_2Fe_{17} were considered.

The optimized phase diagram of the Fe-Er system is presented in Fig. 18 along with experimental data. Meyer[81] used both DTA and quenching experiments followed by XRD and metallographic (OM) phase analysis. It was noted that when Er amount exceeded 0.4 mol fraction, alloy samples reacted with the alumina crucible at elevated temperatures. In general, the melting points of the compounds reported by Meyer[81] were significantly lower than other studies. As stated by Buschow and Van Der Goot,[82] this could result from the reduction of the crucible materials (Al_2O_3) by liquid Er during the experiment. Therefore, Buschow and Van Der Goot[82] used a larger amount of sample than Meyer[81] for the DTA experiment using Al_2O_3 crucible to minimize the composition change. The presences of four compounds in the binary system were confirmed by XRD and OM. $ErFe_2$ was reported to have a congruent melting at 1360 °C, whereas $ErFe_3$, Er_6Fe_{23}, and $Er_{17}Fe_2$ were reported to have peritectic meltings at 1345, 1330, and 1355 °C, respectively. Koleshnikov et al.[83] conducted experiments for the Fe-Er system using DTA and reported liquidus similar to the results of Buschow and Van der Goot[82] except for $ErFe_3$ and $ErFe_2$. They claimed that $ErFe_3$ melted congruently and $ErFe_2$ melted incongruently, which is contradictory to the results of Buschow and Van der Goot.[82] No mutual solubility of Fe and Er was reported in any investigation.

No experimental enthalpy of mixing for liquid Fe-Er system is available. The optimized enthalpy of mixing of the Fe-Er liquid at 1833 K from this study is depicted in Fig. 19 along with the Miedema prediction published by Zhou.[80] Similar to the Fe-Ho system, the enthalpy of mixing in liquid Fe-Er solution was estimated based on the periodic trend of the Fe- heavy RE system, as presented in Fig. 19: $\Delta H_{mix,\text{Fe-Er}} = \Delta H_{mix,\text{Fe-Dy}} + 0.5(\Delta H_{mix,\text{Fe-Lu}} - \Delta H_{mix,\text{Fe-Dy}})$, based on the experimental results of Fe-Dy and Fe-Lu.[52] The predicted value for the present system from the Miedema method[80] is similar to the experimental value of the Fe-Tb system (see Fig. 6), and the value is much positive than the estimated value based on the systematic trend of the enthalpy of mixing in the Fe-RE system.

The ΔH^o_{298} of compounds was measured by Norgren et al.,[71] Gozzi et al.[65] and Meschel et al.[55] These results are plotted in Fig. 20 along with the previous optimization by Zhou et al.[80] Norgren et al.[71] measured the ΔH^o_{298} of $ErFe_2$ and $ErFe_3$ to be -12.5 ± 1.4 and -7.9 ± 1.4 in kJ mol-atom^{-1}, respectively, using the SC-Al at 1100 K.

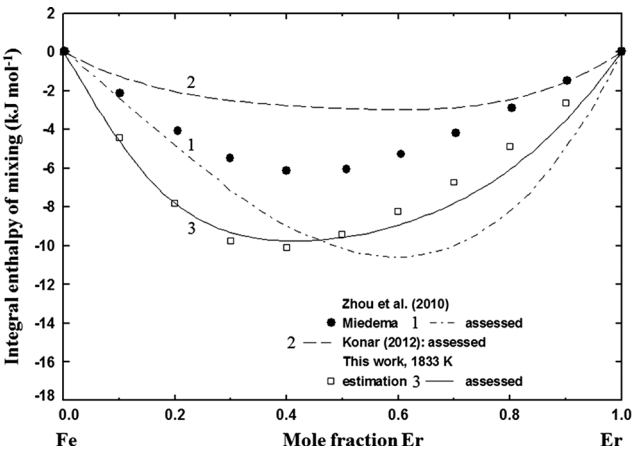

Fig. 19 Integral enthalpy of mixing in Fe-Er liquid at 1833 K with assessments[41,80]

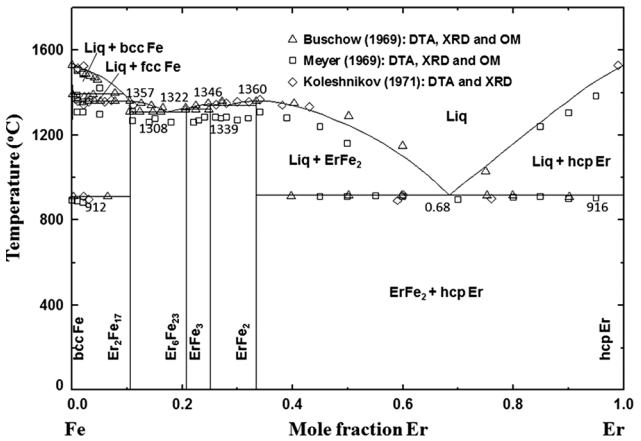

Fig. 18 The optimized phase diagram of the Fe-Er system with the experimental data[81–83]

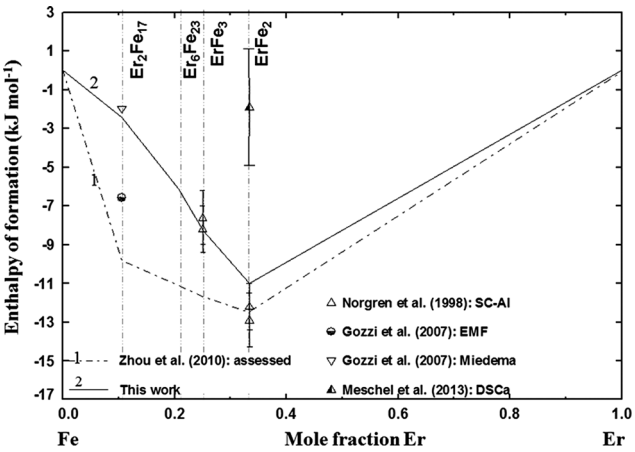

Fig. 20 Enthalpy of formation at 298 K (ΔH^o_{298}) of the intermetallic Fe-Er compounds compared to the experimental data[55,65,71]

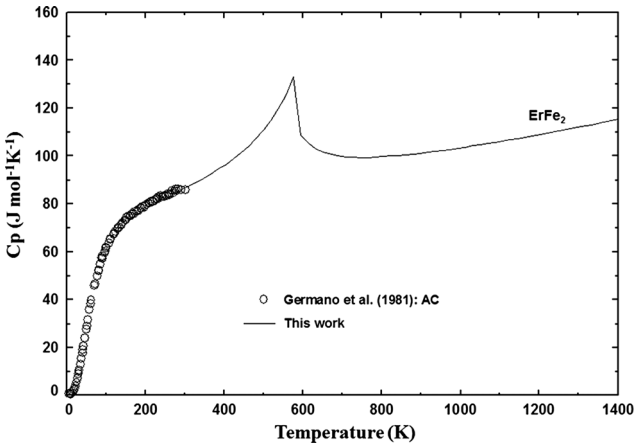

Fig. 21 The optimized C_p of $ErFe_2$ along with the experimental data[57]

Gozzi et al.[65] conducted Miedema calculation and EMF measurements and reported the ΔH^o_{298} for Er_2Fe_{17}. Meschel et al.[55] performed DSCa of the $ErFe_2$ in a BN crucible.

The low-temperature C_p of $ErFe_2$ was reported by Germano et al.[57] using AC in the temperature range of 15-300 K, as shown in Fig. 21. The S^o_{298} of $ErFe_2$ was calculated to be 133.79 J mol^{-1} K^{-1}. The high-temperature C_p was estimated using the N–K rule with a small modification of the temperature-independent term to have continuity with experimental low-temperature C_p. Meschel et al.[55] also reported enthalpy change ($H_{1373} - H_{298}$) to be 34.8 ± 1.7 kJ mol-atom^{-1} as part of their calorimetric experiment, which is calculated to be 37.52 kJ mol-atom^{-1} from the present evaluated C_p. Similarly, the C_p functions for $ErFe_3$, Er_6Fe_{23} and Er_2Fe_{17} were estimated from the N–K rule. The magnetic properties of all compounds were taken from literature.[66,67,78]

In the present optimization, the estimated enthalpy of mixing of the liquid phase in Fig. 19 and ΔH^o_{298} of compounds by Norgren et al.[71] were considered along with phase diagram data to optimize the model parameters of all phases. The liquid was described by using seven parameters including two temperature dependent terms. Enthalpies of formation of the compounds $ErFe_2$ and $ErFe_3$ were optimized to be −11.0 and −8.26 kJ mol-atom^{-1}, respectively, compared to the results (−12.2 ± 1.2 and −8.2 ± 1.2 kJ mol-atom^{-1}, respectively) by Norgren et al. The optimized S^o_{298} of $ErFe_2$ is 128.27 J mol^{-1} K^{-1} which is slightly lower than the experimentally determined value of 133.79 J mol^{-1} K^{-1}. The S^o_{298} of other compounds were optimized by the slight modification from the values obtained from the N–K rule. The overall experimental phase diagram data was well reproduced in the present optimization. The optimized invariant reactions are compared with experimental data in Table 7. All invariant reactions in this study are in good agreement with the results from Buschow and Van der Goot[82] except $ErFe_3$. There is inconsistency in the melting behavior of $ErFe_3$: incongruent melting by Buschow and Van der Goot[82] and congruent melting by Koleshnikov et al.[83] It was very difficult to reproduce the incongruent melting of $ErFe_3$ with simultaneous reproduction of all other data. It should be also noted that $X^5_{\text{Fe-Fe}}$ parameter in the liquid phase was introduced to reproduce the peritectic melting of Er_2Fe_{17}.

The previous assessment by Zhou et al.[80] put the emphasis on the phase diagram data by Buschow and Van der Goot.[82] However, as depicted in Fig. 19, the enthalpy of mixing of Fe-Er liquid assessed by Zhou et al. has the minimum enthalpy of mixing in the Er-rich side, which is most probably wrong from the systematic change in the enthalpy of mixing of the Fe-RE system. They used a large temperature dependent term in liquid parameters, and the ΔH^o_{298} of Er_2Fe_{17} was too negative (about −10 kJ mol-atom^{-1}) compared to the experimental data, as shown in Fig. 20, and the assessed value of S^o_{298} for $ErFe_2$ is 149.53 J mol^{-1} K^{-1} which is much larger than the experimental value[57] of 133.79 J mol^{-1} K^{-1}.

3.6 The Fe-Tm (Iron-Thulium) System

The system was reviewed by Kubaschewski[42] and Okamoto,[84] and thermodynamically assessed by Konar[41] and Kardellass et al.[85] Four stable compounds $TmFe_2$, $TmFe_3$, Tm_6Fe_{23}, and Tm_2Fe_{17} were considered in this system.

The thermodynamic and magnetic properties of the solid and liquid phases are presented in Table 2 and the invariant reactions are presented in Table 8. The phase diagram of the Fe-Tm system is shown in Fig. 22. Kolesnichenko et al.[86] investigated this phase diagram using TA followed by XRD and OM phase analysis but did not mention the detailed experimental procedure in the paper. $TmFe_2$ and Tm_6Fe_{23} with cubic structure and $TmFe_3$ and Tm_2Fe_{17} with hexagonal structure were found as intermetallic compounds. $TmFe_2$ was reported to melt congruently at 1300 °C, while $TmFe_3$ and Tm_6Fe_{23} melted incongruently. Tm_2Fe_{17} was assumed to melt incongruently without strong experimental evidence. The mutual solubility of Fe and Tm has not been investigated, but it is expected to be nearly zero as can be seen in neighboring Fe-RE system such as the Fe-Er and Fe-Lu systems.

No enthalpy of mixing was experimentally investigated. In the present study, the enthalpy of mixing was estimated from the experimental data of the adjacent Fe-Ho and Fe-Er systems: $\Delta H_{mix,\text{Fe-Tm}} = \Delta H_{mix,\text{Fe-Dy}} + 0.75\,(\Delta H_{mix,\text{Fe-Lu}} - \Delta H_{mix,\text{Fe-Dy}})$, as presented in Fig. 23. It should be noted that the calculated enthalpy of mixing from the previous

Table 7 Calculated invariant reactions with the experimental data in the Fe-Er system

Type	Reaction	Composition (X_{Er} in liquid)	T, °C	References
Peritectic	Liq + fcc Fe → Er_2Fe_{17}	0.106	1357	This work
		0.104(a)	1355	82
		0.118(a)	1295 ± 10	81
		0.151(a)	1350	83
		0.105	1343	80[A]
Eutectic	Liq → Er_2Fe_{17} + Er_6Fe_{23}	0.171	1308	This work
		0.165	1315	82
		0.170	1258 ± 6	81
	Liq → $ErFe_5$(c) + Er_6Fe_{23}	0.170	1310	83
		0.174	1326	80[A]
Peritectic	Liq + $ErFe_3$ → Er_6Fe_{23}	0.202	1322	This work
		0.197(a)	1330	82
		0.196(a)	1261 ± 7	81
		0.200(a)	1345	83
		0.191	1328	80[A]
Congruent	Liq → $ErFe_3$	0.250	1346	This work
			1380	83
Eutectic	Liq → $ErFe_2$ + $ErFe_3$	0.279	1339	This work
Peritectic(b)	Liq + $ErFe_2$ → $ErFe_3$	0.248(a)	1345	82
		0.227(a)	1275 ± 10	81
		0.240	1338	80[A]
Congruent	Liq → $ErFe_2$	0.333	1360	This work
			1360	82
			1300 ± 10	81
			1359	80[A]
Peritectic(b)	Liq + $ErFe_3$ → $ErFe_2$	0.376(a)	1355	83
Eutectic	Liq → $ErFe_2$ + hcp Er	0.684	916	This work
		0.700	914	82
		0.700	905 ± 10	81
		0.700	895	83
		0.692	912	80[A]

(a) Extracted from the original phase diagram. (b) The previous authors assumed peritectic meltings of Er_2Fe_{17}, $ErFe_3$ and $ErFe_2$ instead of the congruent melting. (c) The original compounds had different stoichoiometry which was later changed. A: Assessment

assessment by Kardellass et al.[85] show the unmixing trend, which is most probably incorrect considering the enthalpy trend of the Fe-RE system.

Meschel et al.[55] measured the ΔH^o_{298} of $TmFe_2$ to be -2.2 ± 2.8 kJ mol-atom^{-1} using the DSCa, and the result is plotted in Fig. 24. The low-temperature C_p of $TmFe_2$ was measured by Germano et al.[57] using AC. The S^o_{298} of $TmFe_2$ derived from the C_p data is 127.55 J mol^{-1} K^{-1}. The high-temperature C_p was estimated using the N–K rule with a slight adjustment of temperature independent term to make the continuity from the experimentally measured low-temperature C_p. The magnetic contributions to heat capacity were taken from Buschow.[66] The C_p of $TmFe_2$ is presented in Fig. 25. Meschel et al.[55] also measured the heat content change, $H_{1373} - H_{298}$ to be 44.0 ± 1.8 kJ mol-atom^{-1}. According to the evaluated C_p data in Fig. 25, the heat content is calculated to be 36.45 kJ mol-atom^{-1}. The heat capacities of other compounds were also estimated using the N–K rule with the consideration of the magnetic transition,[66] and ΔH^o_{298} and S^o_{298} of the compounds were optimized to reproduce the phase diagram data.

In the present optimization, the estimated enthalpy of mixing and experimental phase diagram data was mainly taken into account to obtain the model parameters of liquid phase first. The Gibbs energy of solid compounds was optimized to reproduce their melting temperature. The optimized ΔH^o_{298} of $TmFe_2$ is -11.23 kJ mol-atom^{-1} which is more negative than the experimental value of -2.2 ± 2.8 kJ mol-atom^{-1} determined by Meschel

Table 8 Calculated invariant reactions with the experimental data in the Fe-Tm system

Type	Reaction	Composition (X_{Tm} in liquid)	T, °C	References
Peritectic	Liq + fcc Fe → Tm_2Fe_{17}	0.125	1307	This work
		0.148(a)	1300	86
		0.110	$1294^{M}/1292^{NM}$	85^{A}
Eutectic	Liq → Tm_2Fe_{17} + Tm_6Fe_{23}	0.177	1255	This work
		0.170	1255	86
		0.176	$1260^{M}/1261^{NM}$	85^{A}
Peritectic	Liq + $TmFe_3$ → Tm_6Fe_{23}	0.205	1264	This work
		0.217(a)	1270	86
		$0.195^{M}/0.199^{NM}$	$1264^{M}/1266^{NM}$	85^{A}
Congruent	Liq → $TmFe_3$	0.250	1284	This work
Eutectic	Liq → $TmFe_3$ + $TmFe_2$	0.278	1278	This work
Peritectic(b)	Liq + $TmFe_2$ → $TmFe_3$	0.225(a)	1280	86
		$0.242^{M}/243^{NM}$	1276	85^{A}
Congruent	Liq → $TmFe_2$	0.333	1300	This work
			1300	86
			$1303^{M}/1302^{NM}$	85^{A}
Eutectic	Liq → $TmFe_2$ + hcp Tm	0.672	941	This work
		0.740	937	86
		0.753	$909^{M}/908^{NM}$	85^{A}

(a) Extracted from the original phase diagram. (b) The previous authors assumed peritectic meltings of Tm_2Fe_{17} and $TmFe_3$ instead of the congruent melting. M: Magnetism of phases considered. NM: Magnetism of phases not considered. A: Assessment

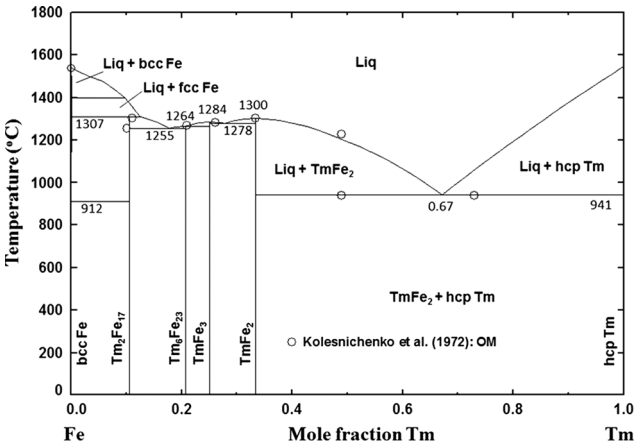

Fig. 22 The optimized phase diagram of the Fe-Tm system with the experimental data[86]

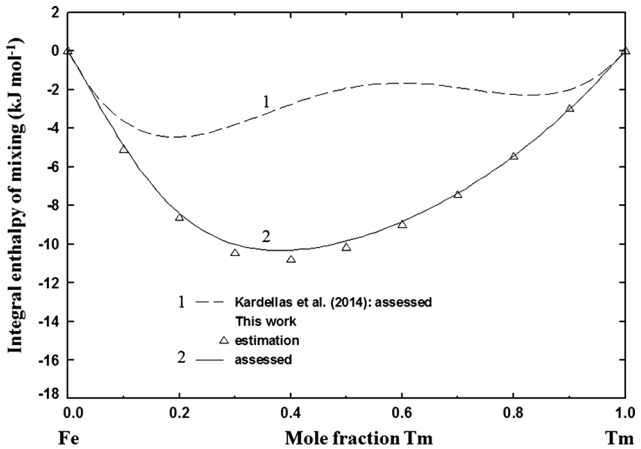

Fig. 23 Integral enthalpy of mixing in Fe-Tm liquid at 1833 K with assessments[85]

et al.[55] However, it should be noted that the ΔH^{o}_{298} of $REFe_2$ measured by Meschel et al.[55] in all other Fe-RE systems tend to be more positive than other experimental data and optimized results in the present study, and also considering the congruent melting of this compound, the ΔH^{o}_{298} of this compound should be the most negative among all intermetallic phases in this system, as in all other Fe-heavy RE systems. Therefore, it is hard to believe the data of Meschel et al. The optimized S^{o}_{298} of $TmFe_2$ is 126.72 J mol^{-1} K^{-1}, consistent with the experimental value of 127.55 J mol^{-1} K^{-1}. All the phase diagram results are well reproduced by the present optimization and the optimized invariant reactions are summarized in Table 8.

The previous thermodynamic assessment by Kardellass et al.[85] was based on phase diagram experiments by Kolesnichenko et al.[86] The excess Gibbs energy of liquid phase was modeled using six parameters including three temperature dependent terms. As shown in Fig. 23, the

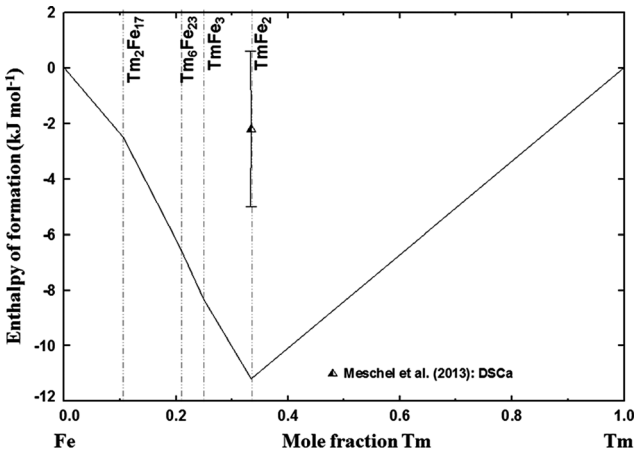

Fig. 24 Enthalpy of formation at 298 K (ΔH^{o}_{298}) of the intermetallic Fe-Tm compounds compared to the experimental data[55]

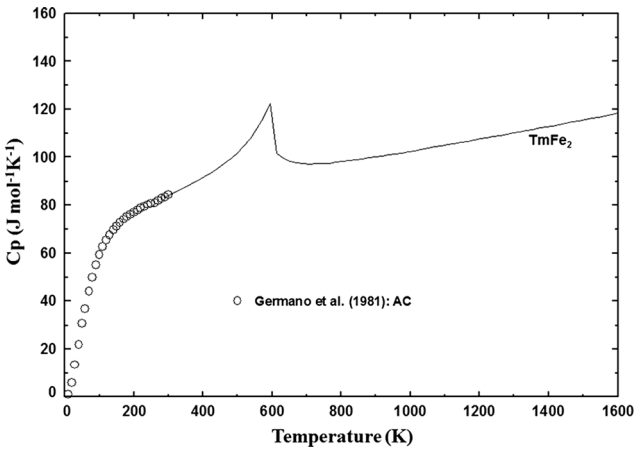

Fig. 25 The optimized C_p of $TmFe_2$ along with the experimental data[57]

assessed enthalpy of mixing had a strange unmixing tendency, which is less plausible. Their high-temperature C_p function for $TmFe_2$ shows discontinuity from the low-temperature C_p data determined by Germano et al.[57] The optimized S^{o}_{298} of $TmFe_2$ is 133.83 J mol^{-1} K^{-1}, which is much larger than experimental value of 127.56 J mol^{-1} K^{-1}.[57]

3.7 The Fe-Lu (Iron-Lutetium) System

The binary Fe-Lu system was reviewed by Kubaschewski[42] and Okamoto,[84] and assessed by Konar[41] and Kardellass et al.[85] The Fe-Lu system has characteristic four intermetallic phases $LuFe_2$, $LuFe_3$, Lu_6Fe_{23}, and Lu_2Fe_{17}. The thermodynamic and magnetic properties of the solid and liquid phases are presented in Table 2 and the invariant reactions are presented in Table 9.

The optimized Fe-Lu phase diagram is presented in Fig. 26. Kolesnichenko et al.[86] investigated this system using TA followed by XRD and OM. Four compounds Lu_2Fe_{17}, Lu_6Fe_{23}, $LuFe_3$, and $LuFe_2$ and bcc Fe, fcc Fe and hcp Lu phases were experimentally found in this system. According to Kolesnichenko et al.,[86] $LuFe_2$ melted congruently at 1345 °C and the remaining compounds $LuFe_3$, Lu_6Fe_{23}, and Lu_2Fe_{17} were formed by peritectic reactions at 1310, 1290, and 1328 °C, respectively. Two eutectic reactions were observed at 970 °C and 0.73 mol fraction Lu and at 1275 °C, and 0.18 mol fraction Lu. No mutual solubility of Fe and Lu has been determined experimentally.

Figure 27 shows the integral and partial enthalpies of liquid measured by Ivanov et al.[52] Ivanov et al.[52] measured the partial enthalpy of mixing using a SC of Fe-rich alloys using zirconia crucible, and Lu-rich alloys using molybdenum crucible at 1950 K. The derived integral enthalpy of mixing shows a minimum at 0.4 mol fraction Lu with a value of -11.56 ± 0.57 kJ mol^{-1}. The Gibbs energy of the liquid phase in the present study is optimized based on these experimental data.

Figure 28 shows the ΔH^{o}_{298} of the compounds in the Fe-Lu system along with the data from Gozzi et al.[65] and Meschel et al.[55] Gozzi et al.[65] conducted Miedema calculation and EMF measurements and reported the ΔH^{o}_{298} for Lu_2Fe_{17}. The ΔH^{o}_{298} of $LuFe_2$ measured by Meschel et al.[55] using DSCa was -3.6 ± 3.1 kJ mol-atom^{-1} which is even lower than that of Lu_2Fe_{17} determined by Gozzi et al. Such a small ΔH^{o}_{298} for $LuFe_2$ is less plausible as discussed above in the previous Fe-Tm system. The low-temperature C_p of $LuFe_2$ and Lu_2Fe_{17} were measured by Germano et al.[57] using AC and Tereshina and Andreev[87] using a Physical Property Measurement System (PPMS) magnetometer device, respectively, as shown in Fig. 29. The high-temperature C_p of both phases were estimated using the N–K rule with a small modification of temperature independent term to have continuity with low-temperature C_p data. The magnetic contributions of both phases were taken from Buschow.[66] As part of their calorimetric measurement, Meschel et al.[55] measured the heat content change $H_{1373} - H_{298}$ of $LuFe_2$. The calculated value from the heat capacity is 35.49 kJ mol-atom^{-1} consistent with experimental value, 32.9 ± 3.1 kJ mol-atom^{-1}. The S^{o}_{298} of $LuFe_2$ and Lu_2Fe_{17} calculated from the low-temperature C_p in Fig. 29 are 107.41 J mol^{-1} K^{-1} and 647.74 J mol^{-1} K^{-1}, respectively. The heat capacities of the other two phases, Lu_6Fe_{23} and $LuFe_3$ were estimated using the N–K rule, and their ΔH^{o}_{298} and S^{o}_{298} were optimized to reproduce the phase diagram data as close as possible.

Seven model parameters including two small temperature dependent terms were used to describe the Gibbs energy of liquid phase. The liquid enthalpy data and phase

Table 9 Calculated invariant reactions with the experimental data in the Fe-Lu system

Type	Reaction	Composition (X_{Lu} in liquid)	T, °C	References
Peritectic	Liq + fcc Fe → Lu_2Fe_{17}	0.111	1329	This work
		0.147(a)	1328	86
		0.090	1320	85[A]
Eutectic	Liq → Lu_2Fe_{17} + Lu_6Fe_{23}	0.172	1273	This work
		0.180(a)	1275	86
		0.158	1276	85[A]
Peritectic	Liq + $LuFe_3$ → Lu_6Fe_{23}	0.202	1287	This work
		0.196(a)	1290	86
		0.183	1287	85[A]
Congruent	Liq → $LuFe_3$	0.250	1310	This work
Eutectic	Liq → $LuFe_3$ + $LuFe_2$	0.263	1309	This work
Peritectic(b)	Liq + $LuFe_2$ → $LuFe_3$	0.225(a)	1310	86
		0.229	1308	85[A]
Congruent	Liq → $LuFe_2$	0.333	1347	This work
			1345	86
			1345	85[A]
Eutectic	Liq → $LuFe_2$ + hcp Lu	0.670	976	This work
		0.730(a)	970	86
		0.741	964	85[A]

(a) Extracted from the original phase diagram. (b) The previous authors assumed peritectic meltings of Lu_2Fe_{17} and $LuFe_3$ instead of the congruent melting. A: Assessment

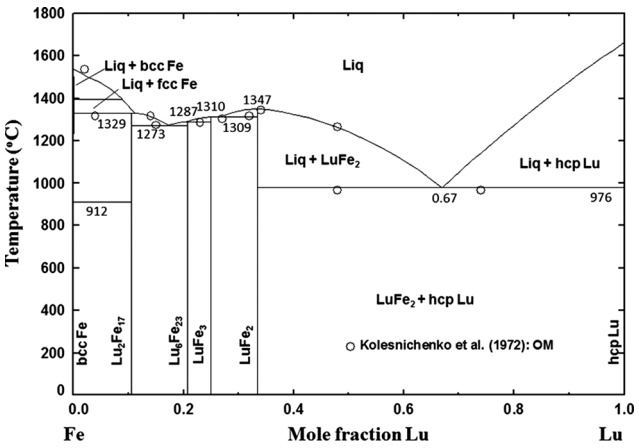

Fig. 26 The optimized phase diagram of the Fe-Lu system with the experimental data[86]

diagram data were simultaneously used to evaluate the Gibbs energy of liquid phase and Gibbs energies of solid compounds. The optimized S^o_{298} of $LuFe_2$ and Lu_2Fe_{17} are 106.6 J mol^{-1} K^{-1} and 646 J mol^{-1} K^{-1}, respectively, which are close to the experimental values of 107.41 J mol^{-1} K^{-1}[57] and 647.74 J mol^{-1} K^{-1},[87] respectively. The optimized ΔH^o_{298} of $LuFe_2$ is −11.77 kJ $mol\text{-}atom^{-1}$ which is much negative than experimental data by Meschel et al.[55] Similar problem of the data for $REFe_2$ by Meschel et al. were pointed out above in the other Fe-RE systems. All invariant reactions by Kolesnichenko et al.[86] were reproduced within ±6 °C in the present optimized diagram except the melting behavior of $LuFe_3$. It was very difficult to reproduce incongruently melting of $LuFe_3$ as reported by Kolesnichenko et al. and it is calculated to melt congruently in the present study. Similar difficulty was witnessed in the Fe-Er and Fe-Tm systems too. The mutual solubilities of Fe and Lu for the terminal fcc, bcc and hcp solid solutions were assumed to be negligible in the present optimization.

The assessed phase diagram by Kardellass et al.[85] can reproduce all experimental invariant reactions. Like the previous Fe-Tm system, however, the critical weakness of the assessment by Kardellass et al.[85] is the unrealistic enthalpy of mixing of liquid Fe-Lu solution as shown in Fig. 27, compared to the experimental data. The C_p functions for $LuFe_2$ and Lu_2Fe_{17} optimized in their study were also inconsistent with experimental C_p data. In their assessment, a homogeneity range was introduced to the compounds Lu_2Fe_{17} and Lu_6Fe_{23} without strong experimental evidence.

3.8 The Fe-Y (Iron-Yttrium) System

The Fe-Y system has been reviewed by Gschneidner[88] and Zhang et al.[89] and assessed by Du et al.,[90] Konar,[41] Lu et al.[91] and Kardellass et al.[92] The crystal structures of the intermetallic phases considered in the present assessment are tabulated in Table 1. The optimized thermodynamic and magnetic parameters of the solid and

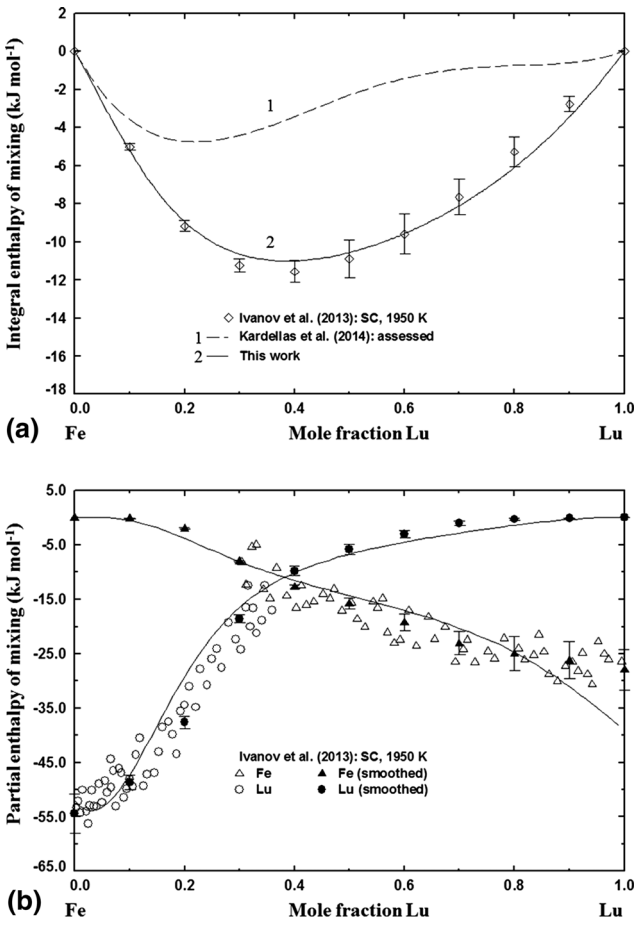

Fig. 27 Enthalpy of mixing in the Fe-Lu system at 1950 K along with the experimental data[52] and assessments[85] (a) Integral enthalpy of mixing and (b) partial enthalpy of mixing

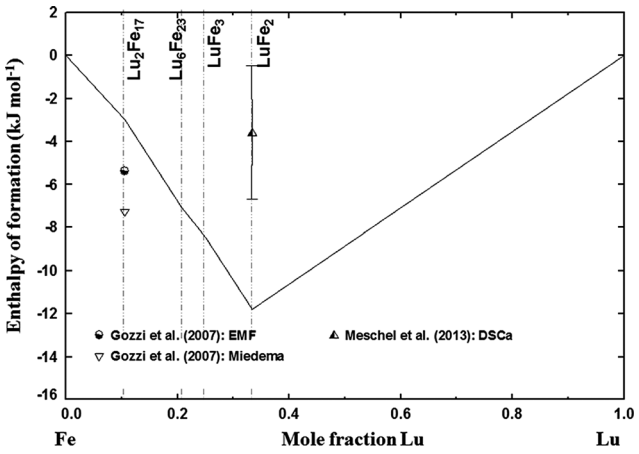

Fig. 28 Enthalpy of formation at 298 K (ΔH^{o}_{298}) of the intermetallic Fe-Lu compounds compared to the experimental data[55]

liquid phases are listed in Table 2 and the invariant reactions are summarized in Table 10.

The optimized binary phase diagram of the Fe-Y system is presented in Fig. 30. The binary phase diagram was

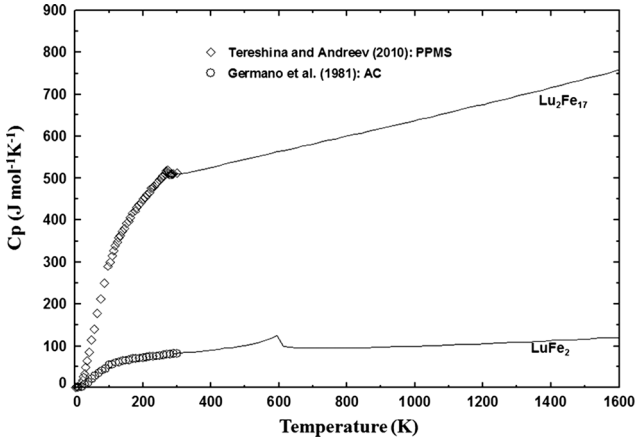

Fig. 29 The optimized C_p of $LuFe_2$ and Lu_2Fe_{17} along with the experimental data[57,87]

investigated by Farkas and Bauer,[93] Domagala et al.,[94] and Nagai et al.[72] Farkas and Bauer[93] studied the Fe-rich side (up to 30 wt.% Y) by TA. The presence of YFe_5 and YFe_4 was analyzed by XRD and OM. The phase equilibria and the transition temperatures were also measured by Farkas and Bauer. But due to the high heating/cooling rate of 400 °C min^{-1} in the TA, severe undercooling was introduced. Therefore, their data cannot be used in the present study. Domagala et al.[94] used visual melting observation and quenching experiment followed by OM and XRD phase analysis. A eutectic reaction (Liq → hcp Y + YFe_2) was found at 0.65 mol fraction Y at 900 °C. With the help of XRD analysis, the polymorphic transition from hcp Y to bcc Y at 1478.5 °C and melting point of Y was revealed. Domagala et al. reported congruent meltings of YFe_3, YFe_4, and YFe_9, but the incongruent melting of YFe_2. As part of the thermodynamic study by Nagai et al.[72] using KEMS, the phase transition was identified from the measured activity change at 1200-1300 °C. The mutual solid solubility of Fe and Y is shown in Fig. 30(b) and (c). Domagala et al.[94] measured the solubility by XRD measurement and reported the terminal solubilities of 0.015 mol fraction of Fe in Y at 900 °C, and 0.066 mol fraction solubility of Y in Fe at 1350 °C. Li and Xing[95] conducted EPMA to determine the solubility of Y in bcc Fe from 600 to 880 °C.

Ryss et al.[96] and Sudavtsova et al.[97] measured the partial enthalpy of mixing of liquid Fe-Y solution using SC at 1873 and 1870 K, respectively, and derived the integral enthalpy of mixing, as shown in Fig. 31(a) and (b). Ryss et al. suggested that the minimum of the integral enthalpy of mixing is about −8.144 kJ mol^{-1} at 0.47 mol fraction Y. Sudavtsova et al. conducted SC in the Fe-rich side of the Fe-Y liquid under He atmosphere. The partial enthalpy of mixing of Y in the Fe-rich side determined by Sudavtsova et al. is more positive than that of Ryss et al. In the present

Table 10 Calculated invariant reactions with the experimental data in the Fe-Y system

Type	Reaction	Composition (X_Y in liquid)	T, °C	References
Peritectic	Liq + bcc Fe → fcc Fe	0.039	1452	This work
		0.013	1400 ± 25	94
		$0.048^{K}/0.048^{RK}$	$1391^{K}/1390^{RK}$	85[A]
Eutectic	Liq → fcc Fe + Y_2Fe_{17}	0.069	1384	This work
	Liq + fcc Fe → YFe_9^+	0.082(a)	1350 ± 25	94
	Liq → fcc Fe + Y_2Fe_{17}	0.072	1390^{K}	85[A]
	Liq → fcc Fe + Y_2Fe_{17}	0.056	1360^{RK}	85[A]
Congruent	Liq → Y_2Fe_{17}	0.105	1406	This work
	Liq → YFe_9^+	0.100	1400 ± 25	94
	Liq → Y_2Fe_{17}	0.105	$1399^{K}/1403^{RK}$	85[A]
Eutectic	Liq → Y_6Fe_{23} + Y_2Fe_{17}	0.159	1372	This work
	Liq → YFe_4^+ + YFe_9^+	0.128	1280	94
	Liq → Y_6Fe_{23} + Y_2Fe_{17}	0.179/0.182	$1365^{K}/1332^{RK}$	85[A]
Congruent	Liq → Y_6Fe_{23}	0.207	1394	This work
	Liq → YFe_4^+	0.200	1300	94
	Liq → Y_6Fe_{23}	0.207	$1368^{K}/1333^{RK}$	85[A]
Eutectic	Liq → Y_6Fe_{23} + YFe_3	0.210	1394	This work
	Liq → YFe_4^+ + YFe_3	0.236	1250	94
	Liq → Y_6Fe_{23} + YFe_3	0.216/0.207	$1367^{K}/1332^{RK}$	85[A]
Congruent	Liq → YFe_3	0.250	1408	This work
			1400	94
			$1374^{K}/1350^{RK}$	85[A]
Peritectic	Liq + YFe_3 → YFe_2	0.475	1124	This work
		0.424	1125 ± 25	94
		0.482/0.443	$1124^{K}/1136^{RK}$	85[A]
Eutectic	Liq → YFe_2 + hcp Y	0.601	883	This work
		0.653	900 ± 10	94
		0.637/0.612	$845^{K}/873^{RK}$	85[A]
Metatectic	bcc Y → hcp Y + Liq	0.978	1479	This work
		$0.976^{K}/0.979^{RK}$	$1476^{K}/1477^{RK}$	85[A]

(a) Extracted from the original phase diagram. K: Kaptay's formalism, RK: Redlich–Kister formalism, A: Assessment

optimization, the enthalpy of mixing data by Ryss et al. was more weighted than the results of Sudavtsova et al.

The ΔH^o_{298} of the compounds were estimated by Van Mal et al.[98] and Watson and Bennet.[99] Van Mal et al. predicted the ΔH^o_{298} of the compounds based on Miedema's theory.[98] Watson and Bennet developed a simple electron band theory model which can predict the ΔH^o_{298} of the intermetallic phases of metals with d and/or f bands. Gozzi et al.[65] reported the ΔH^o_{298} of the Y_2Fe_{17} phase, derived from the Gibbs energy of formation determined using galvanic cells with CaF_2 electrolyte, to be −8.7 kJ mol-atom^{-1}. As seen in the above Fe-RE systems, the ΔH^o_{298} of RE_2Fe_{17} measured by Gozzi et al.[65] is typically much negative than the experimental data and also optimized values in the present study. As no other experimental ΔH^o_{298} are available in the literature, the enthalpy was modeled based on the Gibbs energy of formation of the Fe-Y compounds measured by Subramaniam and Smith,[100] as depicted in Fig. 32(a) and (b). Subramaniam and Smith[100] employed EMF technique with solid electrolyte to determine the Gibbs free energy of four intermetallic phases over the temperature range between 620 and 998 °C. Their results of the Gibbs energy of formation and derived enthalpy and entropy of formation from the elements at 973 K are plotted in Fig. 32.

The C_p of YFe_2 from 300 to 600 K was measured by Dariel et al.[101] to determine Curie temperature using DSC. However, actual C_p data were not given in the paper except for the Curie temperature at 535 K. The low-temperature C_p of Y_2Fe_{17} was measured by Mandal et al.[102] with a PPMS device, as presented in Fig. 33. The S^o_{298} derived from this result is 660.71 J mol^{-1} K^{-1}. In the

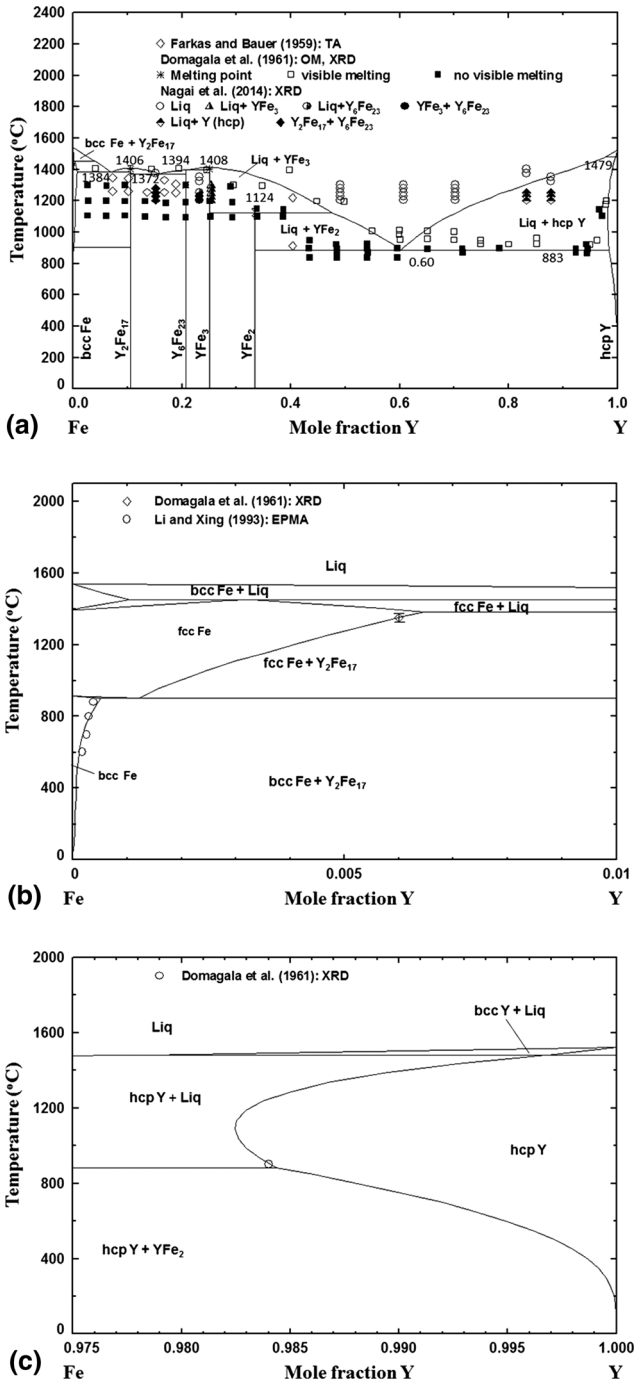

Fig. 30 The optimized phase diagram of the Fe-Y system with the experimental data (a) Overall composition range,[72,93,94] (b) in the Fe-rich side,[94,95] and (c) in Y rich side[94]

present study, the high-temperature C_p function of Y_2Fe_{17} was obtained by the N–K rule with a slight modification of the temperature independent term to have continuity with the low-temperature C_p. It should be noted that the ΔS_{973} calculated from the C_p of Y_2Fe_{17} in Fig. 33 is inconsistent with the results of Subramaniam and Smith[100] in Fig. 32(c). This casts doubt on the accuracy of the EMF

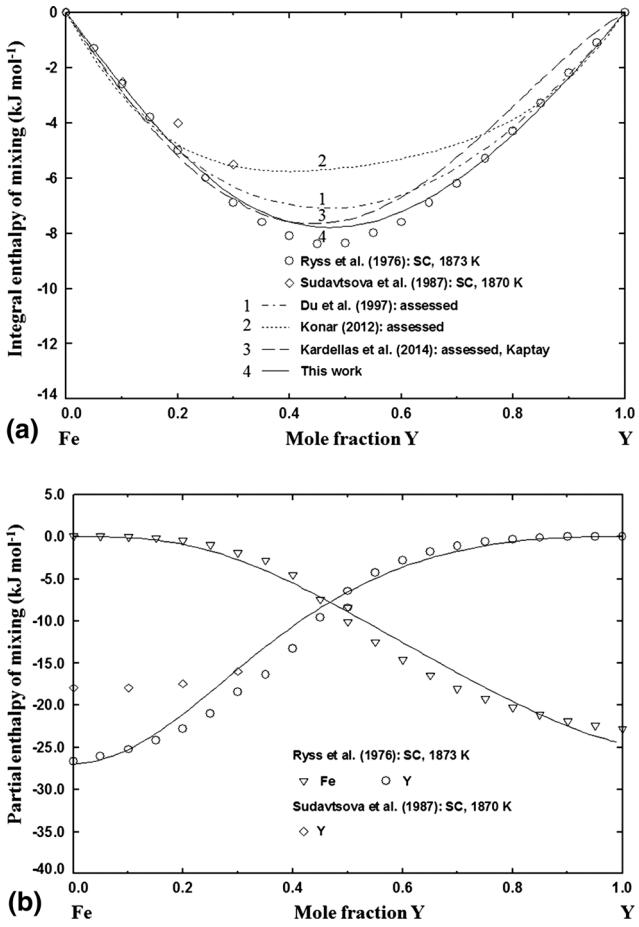

Fig. 31 Enthalpy of mixing in the Fe-Y system at 1873 K along with experimental data[96,97] and assessments[41,90,92] (a) Integral enthalpy of mixing and the previous optimization and (b) partial enthalpy of mixing

results of Subramaniam and Smith. The C_p functions of other compounds were also obtained using the N–K rule. The magnetic contributions to C_p functions obtained by several researchers[103–106] are listed in Table 2.

The activities of Fe and Y at 1473 and 1573 K were derived by Nagai et al.[72] from their KEMS experiment, as shown in Fig. 34. Owing to the high affinity of Y containing alloys to oxygen, they were stored under spindle oil. Oxygen amount of alloys in pre and post experiment was minimal, as determined by inert gas fusion-infrared absorptiometry. The KEMS measurements were carried out for the samples across the entire composition in the temperature range of 1473-1573 K. The ion currents for Y were determined with the help of ^{89}Y isotope. The more abundant ^{54}Fe and ^{56}Fe were chosen for Fe detection among the possible ^{54}Fe, ^{56}Fe, ^{57}Fe and ^{58}Fe isotopes. As can be seen in Fig. 34, the activity of Y shows a large negative deviation from ideal solution behavior in Y rich side, which seems to be too negative compared to the rest of liquid Fe-RE solution. This will be discussed again below.

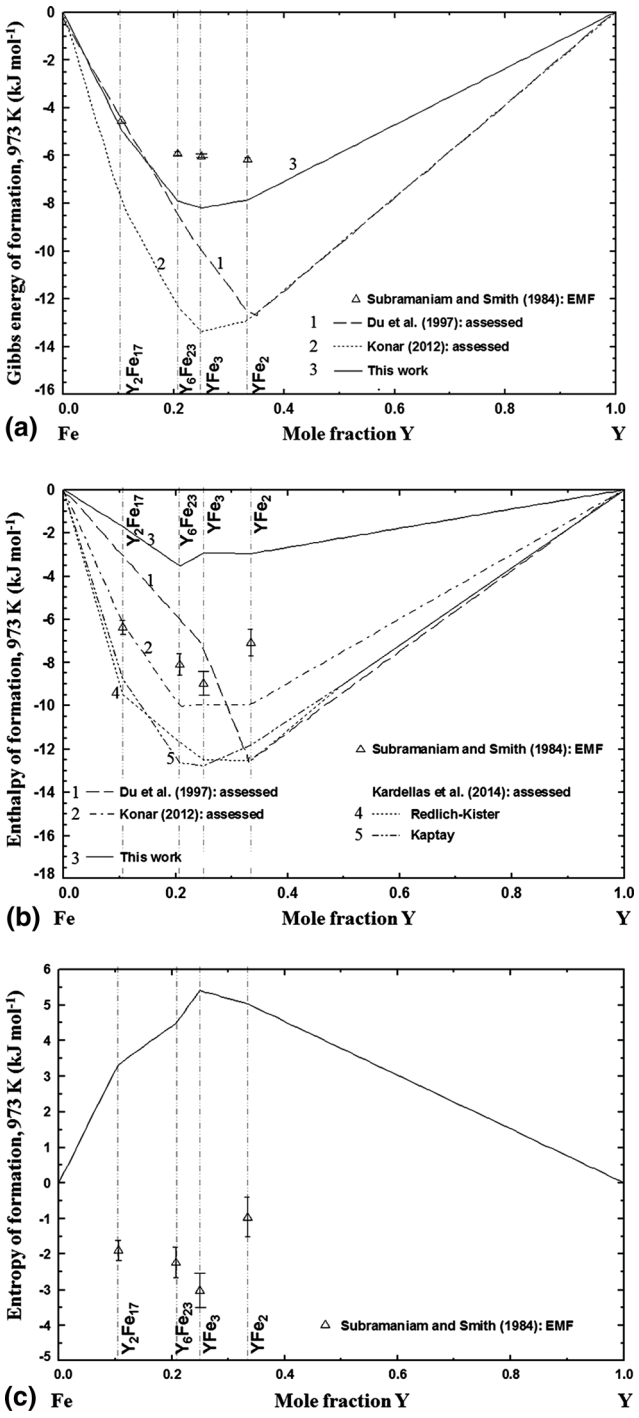

Fig. 32 Thermodynamic properties of the Fe-Y compounds with experimental data[100] and assessments,[41,90,92] (a) Gibbs energy of formation of compounds at 973 K, (b) Enthalpy of formation at 973 K and (c) Entropy of formation of compounds at 973 K

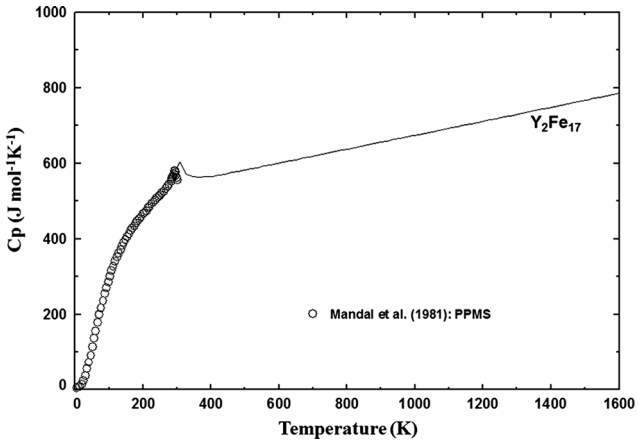

Fig. 33 Low-temperature heat capacity of Y_2Fe_{17}[102]

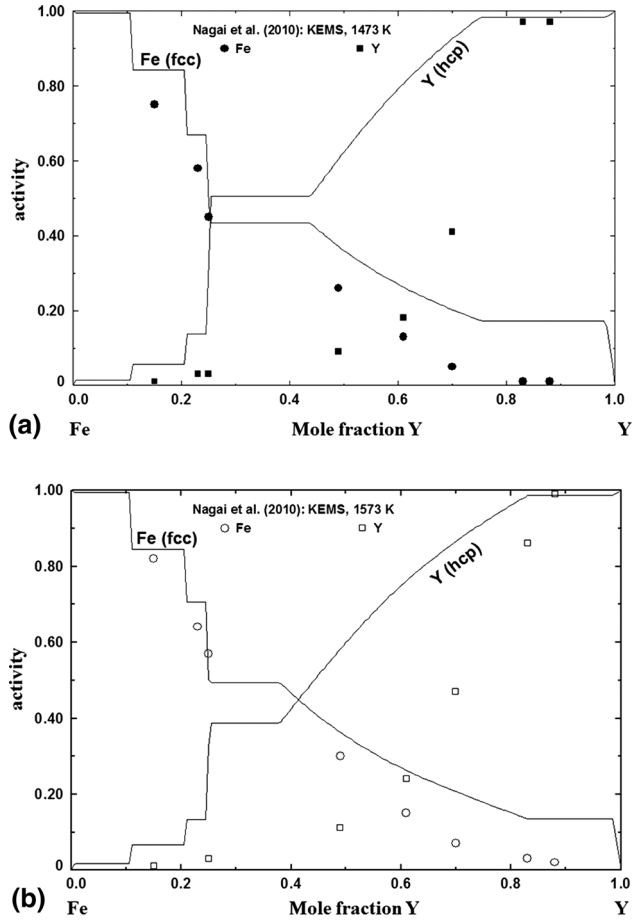

Fig. 34 The activity of Fe and Y at (a) 1473 K and (b) 1573 K with the experimental data[72]

In the present study, the enthalpy of the liquid phase, Gibbs energy of solid compounds and low-temperature C_p (S^o_{298}) of Y_2Fe_{17} were simultaneously considered along with phase diagram information to optimize the thermodynamic parameters of solid and liquid phases. The enthalpy of mixing and partial enthalpy of liquid phase were well reproduced. The optimized S^o_{298} value of Y_2Fe_{17} in the present work is 623.0 J mol^{-1} K^{-1}, which is within 5% error from experimental value of 660.71 J mol^{-1} K^{-1} from low-temperature C_p.[102] It should be noted that if the experimental S^o_{298} (660.71 J mol^{-1} K^{-1}) is used, a larger

error will be obtained in the entropy of formation in Fig. 32(c). The calculated formation Gibbs energies, enthalpies, and entropies of compounds at 983 K from the present study are plotted in Fig. 32 along with the experimental data of Subramaniam and Smith.[100] The calculated Gibbs energy data from the present study is slightly lower than the experimental values. But the previous assessments[90–92,107] show a much larger deviation from the experimental data. The enthalpy of formation data also shows similar results. In the case of the entropies of formation, the calculated values from the present study are positive as opposed to the negative experimental data. As discussed above, the experimental entropy of formation of Y_2Fe_{17} at 298 K is already positive,[102] and the entropy of formation at 973 K would most probably be positive as calculated from the present data.

The activities of Fe and Y at both 1573 and 1473 K are substantially underestimated. This can be due to an error in the ion current measurements for Fe and Y, and high oxygen contamination of Y. The activities of Y and Fe are also well reproduced at 1473 and 1573 K in the Fe-rich region, while the activity of Y in the Y-rich region is more positive than the experimental results of Nagai et al.[72] In order to reproduce the activity of Y of Nagai et al.[72] in the Y-rich region, more negative Gibbs energy of liquid is required, which results in much lower eutectic temperature for Liq $\rightarrow$ YFe_2 + hcp Y. In the present study, more weight was given to the phase diagram than the KEMS data by Nagai et al.[72] All phase diagram data from Domagala et al.[94] was well reproduced, as shown in Fig. 30(a), except the congruent melting of Y_6Fe_{23}. As mentioned earlier, there is no critical evidence of peritectic melting of this compound. The mutual solubilities of Fe and Y for the terminal fcc, bcc, and hcp solid solutions were reproduced by adding one regular solution model parameter. In the case of the fcc solution, the temperature dependent term was also necessary to reproduce the steep solubility as reported by Domagala et al.,[94] as shown in Fig. 30(b) and (c). All invariant reactions in the binary system are listed in Table 10.

The Fe-Y system has been assessed by Du et al.,[90] Lu et al.[91] and Kardellass et al.[92,107] Du et al.[90] assessed the thermodynamic properties of the liquid and solid phases, where the Gibbs energy of compounds was significantly different from the experimental data in Fig. 32. The Gibbs energy of formation data reported by Subramaniam and Smith[100] was only reproduced for Y_2Fe_{17} and not for Y_6Fe_{23}, YFe_3, and YFe_2. Lu et al.[91] reassessed the modeling conducted by Du et al.[90] All the intermetallic phases were considered to be stoichiometric phases. Neither the thermodynamic parameters for the liquid or solid phases, nor the invariant reactions were given in their paper, so it is hard to evaluate their work. The phase diagram depicted is identical to that assessed from the present study, except no terminal solid solutions were considered. Kardellass et al.[92,107] presented a phase diagram with considerable homogeneity range in the Y_6Fe_{23} and YFe_2 phase without any experimental evidence. Several investigators[108,109] reported the presence of a stoichiometric phase, without any solid solubility of Fe in Y_6Fe_{23}. Kardellass et al.[92,107] did not consider the terminal solid solutions of Y and Fe in their assessment.

4 Discussion and Systematic Analysis

Certainly, there are systematic trends in the thermochemical properties and phase diagrams of the Fe-RE systems. The trends observed in the enthalpy and entropy of liquid phase, the enthalpy and entropy of formation of solid phases, and the phase diagram information in the Fe-RE system will be discussed below.

The optimized enthalpy of mixing of the liquid Fe-RE solution at 1873 K is presented in Fig. 35, which manifests a periodic trend. The enthalpy of mixing for all liquid Fe-RE alloys shows maximum or minimum values at around 0.4 mol fraction RE. It varies systematically from 5.5 to -12 kJ mol^{-1} with increasing atomic number of RE. This systematic change in the mixing enthalpy was taken into account to estimate the enthalpy of mixing of the Fe-Ho, Fe-Er, and Fe-Tm solution, where no experimental data are available. The position of minimum enthalpies of mixing is near 0.4 mol fraction of RE. This asymmetric nature of mixing enthalpy may result from the size difference between Fe and RE: RE has a larger atomic size (r_{La} = 188 pm and r_{Lu} = 173 pm) than Fe (r_{Fe} = 140 pm).[58] It should be noted that the Fe-Y system shows a bit different behavior than other RE systems. A similar trend was observed in the Mn-RE systems[21] where enthalpy of mixing varies from 8 to -8 kJ mol^{-1}. In other binary RE

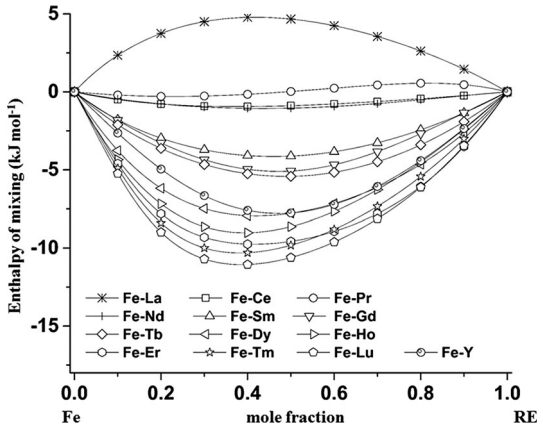

Fig. 35 Comparison of integral enthalpies of liquid Fe-RE at 1873 K

systems, the enthalpies of mixing are already very negative, so it is hard to observe the clear trend in enthalpy of mixing data: for example, the Si-RE alloys (−65 to −75 kJ mol^{-1}),[24] Pb-RE alloys (−40 to −60 kJ mol^{-1}),[26] Al-RE systems (−30 to −40 kJ mol^{-1})[27] and Zn-RE systems (−20 to −32 kJ mol^{-1}).[30]

The optimized ΔH^{o}_{298} and ΔS^{o}_{298} of the binary Fe-RE systems from the respective elements are presented in Fig. 36 and 37, respectively, which also show definitive similarity in trend. The $REFe_2$ compound shows the most negative ΔH^{o}_{298} value of all Fe-RE systems, and also most negative ΔS^{o}_{298}. It should be also noted that the ΔH^{o}_{298} values measured by Meschel et al.[55] are mostly more positive than the optimized values in the present study. Therefore, more investigation into these thermodynamic properties is necessary for future.

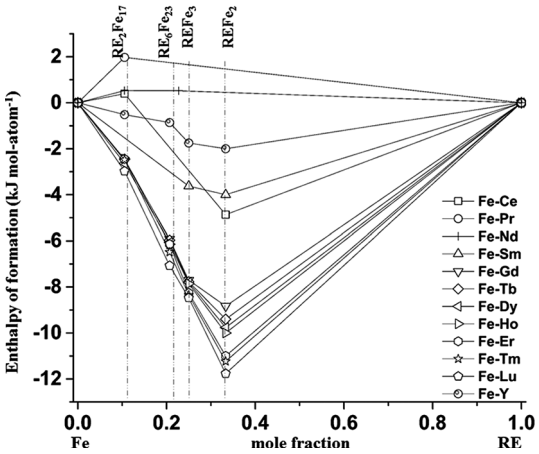

Fig. 36 Comparison of enthalpies of formation of Fe-RE compounds at 298 K. (based on one mole of Fe and RE)

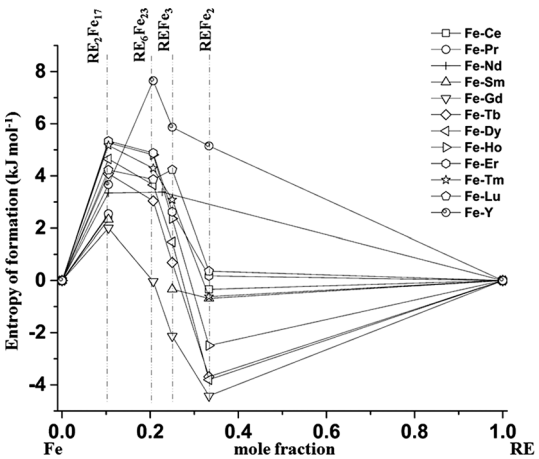

Fig. 37 Comparison of entropies of formation of Fe-RE compounds at 298 K. (based on one mole of Fe and RE) from elemental references

Similarly, a systematic trend is observed in the melting temperatures of the intermetallic compounds. The melting temperatures of the Fe-RE compounds and the eutectic

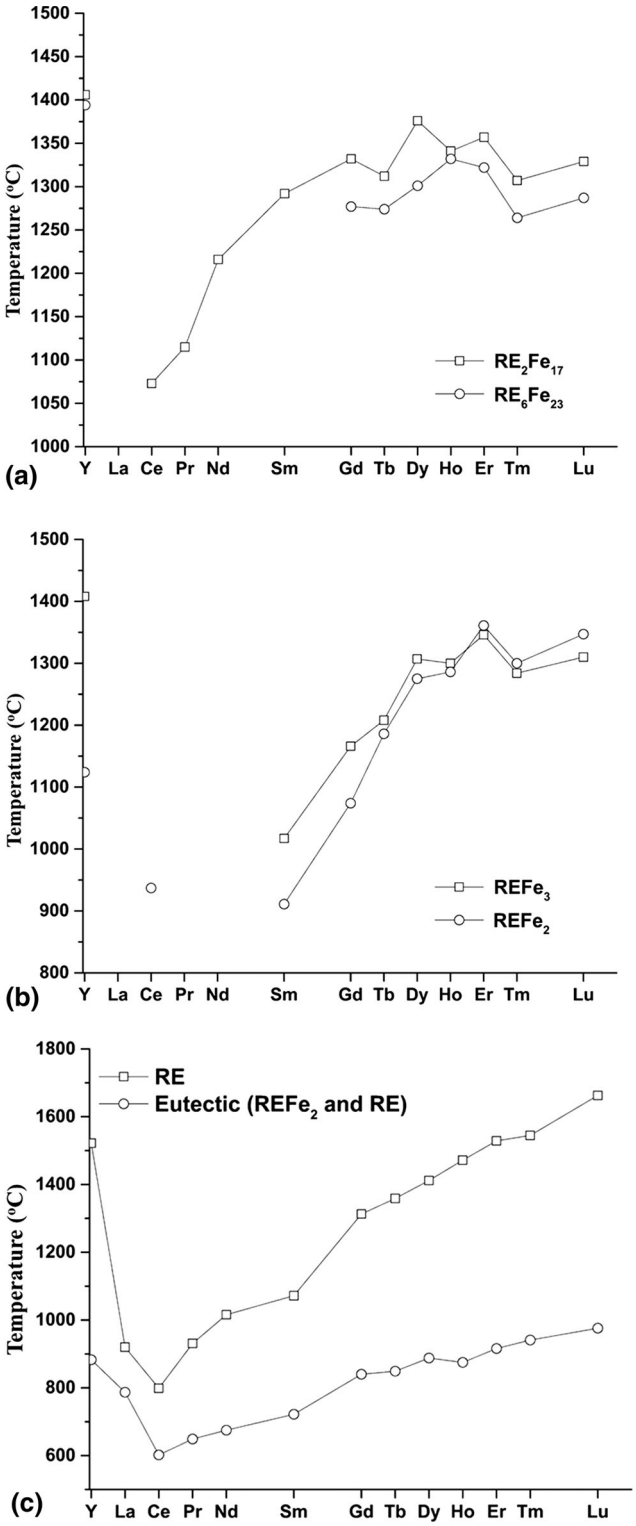

Fig. 38 Systematic changes in the melting temperatures of Fe-RE compounds (a) RE_2Fe_{17} and RE_6Fe_{23}, (b) $REFe_3$ and $REFe_2$ (c) RE melting point and the eutectic temperatures between $REFe_2$ and RE

temperature (eutectic reaction: Liq → $REFe_2$ + RE) is shown in Fig. 38. The melting point of all the compounds is increasing gradually with increasing atomic number of RE. The increase becomes flattened out from Fe-Ho system. The temperature of the eutectic reaction 'Liq → $REFe_2$ + RE' shows a clear increasing trend with increasing atomic number of RE. A similar trend was previously discussed in the Si-RE system.[24,25]

A collection of all the optimized phase diagrams of the Fe-RE systems obtained in the present study and by Konar et al.,[31] is shown in Fig. 39. As can be seen in the collection, no intermetallic phase forms in the Fe-La system, and then RE_2Fe_{17}, $REFe_3$, and $REFe_2$ are gradually forming with increasing atomic number of RE. Additionally, RE_6Fe_{23} compound forms in the heavy RE systems. The melting behavior of intermetallic compounds also changes from peritectic to congruent melting with increasing atomic number of RE. This means that the enthalpy of formation (Gibbs energy of formation) of intermetallic Fe-RE phase becomes more stable (negative) with increasing atomic number of RE, as also seen in the enthalpy of mixing in liquid Fe-RE solution. In the case of the Fe-Er, -Tm, and -Lu systems, however, we found that it is necessary to add positive excess parameters in the Fe-rich liquid solution to reproduce the peritectic melting behavior of RE_2Fe_{17} compounds.

The enthalpy of formation is one of the important thermodynamic properties of solid compounds that determine their thermal stabilities. Amongst the semi-empirical approaches to predict the standard enthalpy of formation (ΔH^{o}_{298}), Miedema model[98,110,111] improved by Zhang et al.[112–114] using statistical approach (ab initio throughput data-mining (HTDM) method) was used in this study for the estimation of enthalpies of formation all the Fe-RE compounds. The semi-empirical nature of this Miedema model comes from the element specific constants such as electronic configuration, electron densities, and atomic radius. In Fig. 40, the optimized enthalpies of formation of

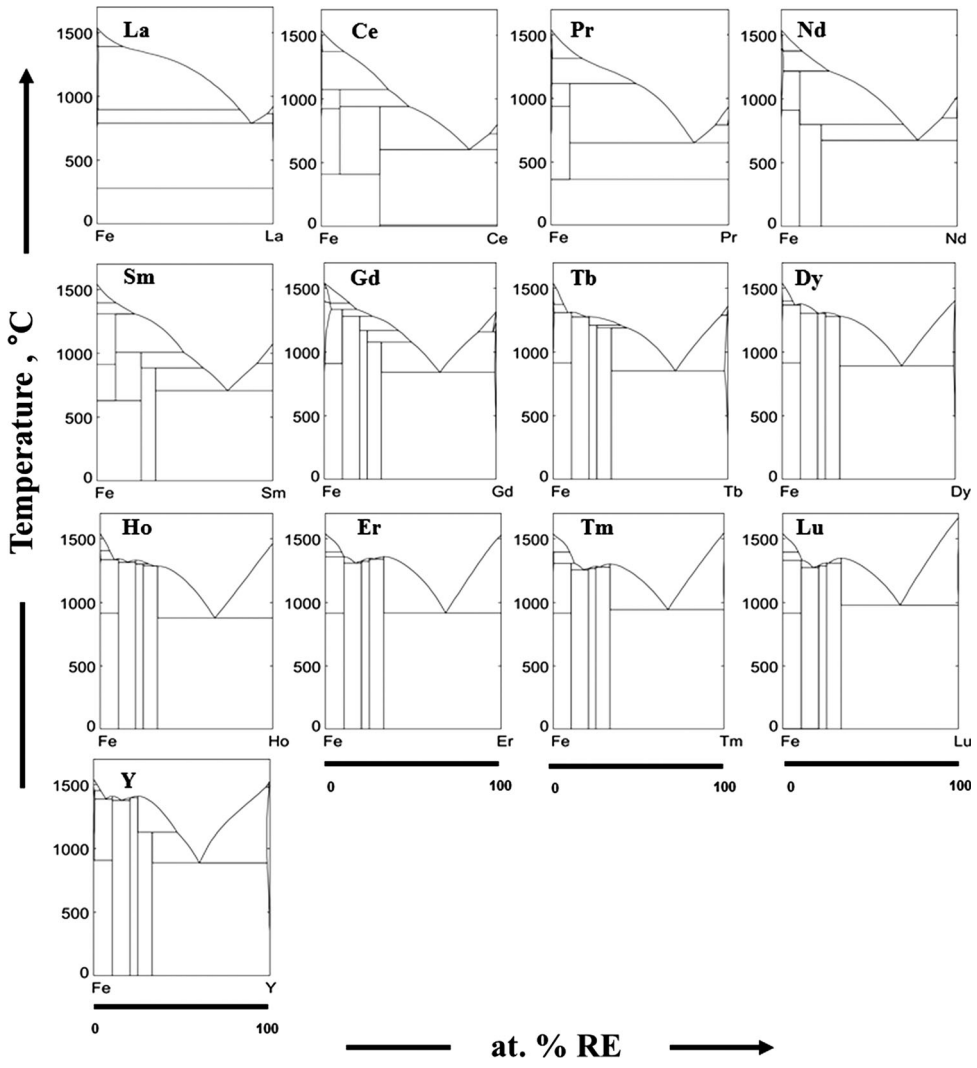

Fig. 39 A collection of the optimized phase diagrams of the Fe-RE systems

all Fe-RE compounds in the present study are compared to those predicted from the Miedema model. In Fig. 40, only the intermetallic compounds in the Fe-heavy RE system was compared as Fe-light RE system has only a few intermetallic compounds. It should be noted that the Miedema results for the compounds in the Fe-Gd and Fe-Y systems would be less reliable because Zhang et al.[111–113] contain the same ionic radius and similar electron density parameter for Gd and Y. Similar incongruences were also observed in the ionic radius and electron density parameter of Ho.

In the previous studies[23,28] on RE containing systems, it was also demonstrated that the prediction from the Miedema model was less accurate for RE containing compounds. Although there are significant differences in the results from present optimization and the Miedema model, the general trend in the formation enthalpy is the same. The enthalpy of formation (per mol-atom) of a given Fe-RE system decreases in the order of RE_2Fe_{17}, RE_6Fe_{23}, $REFe_3$, and $REFe_2$. That is, the minimum of enthalpy of formation in solid state occurs at $REFe_2$. In the case of RE_2Fe_{17}, the enthalpies of formation are not significantly changed with the atomic number of RE, while those of $REFe_2$ are noticeably decreasing with increasing atomic number of RE.

In the present analysis, the general trends of the enthalpies in the solid and liquid state are plotted with the variation of the atomic number of RE. The physical and chemical properties of RE show the systematic changes with the atomic number of RE. For example, the electronegativity and density of RE increase with increasing atomic number of RE. Therefore, the general systematic trends discussed in this study can be also valid with electronegativity and density of RE.

In general, there is a lack of experimental information on the homogeneity range of terminal Fe and RE solid solution. Although it is expected to be small, such solubility should be further investigated for the complete understanding of the phase diagram of the Fe-RE system.

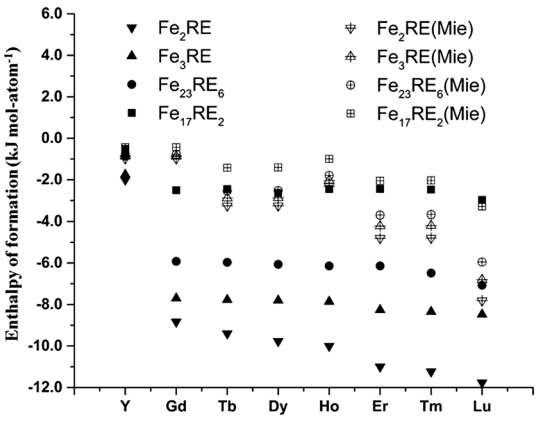

Fig. 40 Comparison of the enthalpy of formation of Fe-RE compounds at 298 K between the optimized results (solid symbols) and predicted results using the Miedema method (empty symbols)[112–114]

5 Conclusions

A critical evaluation and optimization of all available phase diagram and thermodynamic data of the Fe-RE (RE = Gd, Tb, Dy, Ho, Er, Tm, Lu, and Y) systems was conducted to obtain consistent thermodynamic functions of all the phases in each system. The Gibbs energy functions for all stoichiometric compounds were obtained with consideration of their magnetic properties. The liquid Fe-RE phase was described using the MQM and the solid solution phases such as bcc, fcc, and hcp solutions were described using the one-sublattice Compound Energy Formalism.

In the thermodynamic modeling, it is found that the Fe-RE systems show systematic trends in the phase diagrams and thermodynamic properties. In general, the formation enthalpy of intermetallic compounds and enthalpy of mixing of liquid phase become more negative with an increasing atomic number of RE. The melting point of the intermetallic phases increases gradually with increasing atomic number of RE. Such trend was used to estimate unknown thermodynamic properties of several Fe-RE systems, and clarify the melting behavior of compounds. In conclusion, in the present study, a more accurate thermodynamic description of the Fe-RE system is achieved through simultaneous thermodynamic optimization of all Fe-RE systems.

Acknowledgments This project was financially supported by Korea institute of Industrial Technology (KITECH), South Korea.

References

1. V.G. Kravets, L.V. Poperenko, and I.A. Shaikevich, Optical Properties of Iron Alloys with Heavy Rare-Earth Elements, *Sov. Phy. J.*, 1988, **31**(12), p 1007–1010
2. S. Gupta and K.G. Suresh, Review on Magnetic and Related Properties of RTX Compounds, *J. Alloys Compd.*, 2015, **618**, p 562–606
3. J. Li, J. Huo, J. Law, C. Chang, J. Du, Q. Man, X. Wang, and R.-W. Li, Magnetocaloric Effect in Heavy Rare-Earth Elements Doped Fe-Based Bulk Metallic Glasses with Tunable Curie Temperature, *J. Appl. Phys.*, 2014, **116**(6), p 063902
4. K.M. Mukimov, S.M. Sharipov, and L.A. Ernazarova, The Magneto-optical Spectra and Behaviour of the Joint Density of States of the Intermetallic Compounds RFe_2 (R = Gd, Tb, Dy, Ho, Er) and YFe_2, *Phys. Status Solidi B*, 1985, **127**(2), p K129–K131
5. S.M. Sharipov, K.M. Mukimov, and L.A. Ernazarova, The Heavy Rare-Earth Contribution to the Electronic Structure of the RFe_2 and R_2Fe_{17} Intermetallic Compounds, *Phys. Status Solidi (b)*, 1986, **134**(1), p K59–K62

6. N.C. Koon, C.M. Williams, and B.N. Das, Giant Magnetostriction Materials, *J. Magn. Magn. Mater.*, 1991, **100**(1), p 173–185
7. F. Pan, D.V. Edmonds, S. Zhou, and P. Ding, Effects of Rare Earth Metals on Electrical Conductivity and Mechanical Properties of Commercial Purity Aluminium, *Mater. Sci. Technol.*, 1994, **10**(11), p 933–935
8. F. Rosalbino, D. Macciò, E. Angelini, A. Saccone, and S. Delfino, Electrocatalytic Properties of Fe-R (R = Rare Earth Metal) Crystalline Alloys as Hydrogen Electrodes in Alkaline Water Electrolysis, *J. Alloys Compd.*, 2005, **403**(1-2), p 275–282
9. F. Rosalbino, G. Borzone, E. Angelini, and R. Raggio, Hydrogen Evolution Reaction on Ni-RE (RE = Rare Earth) Crystalline Alloys, *Electrochim. Acta*, 2003, **48**(25-26), p 3939–3944
10. K.J. Dormer, R.E. Nordquist, G.L. Richard, and J.V.D. Hough, The Use of Rare-Earth Magnet Couplers in Cochlear Implants, *Laryngoscope*, 1981, **91**(11), p 1812–1820
11. M. Humphries, *Rare Earth Elements: The Global Supply Chain*, DIANE Publishing, Collingdale, 2010
12. J. Ma and F. Liu, Application of Rare Earth Element in Steel and Its Influence on Steel Properties, *Gangtie Yanjiu*, 2009, **37**(3), p 54–56
13. L.A. Smirnov, V.A. Rovnushkin, A.S. Oryshchenko, G.Y. Kalinin, and V.G. Milyuts, Modification of Steel and Alloys with Rare-Earth Elements. Part 1, *Metallurgist*, 2016, **59**(11), p 1053–1061
14. L.A. Luyckx, The Rare Earth Metals in Steel, *Industrial Applications of Rare Earth Elements*, American Chemical Society, Washington, DC, 1981, p 43–78
15. C.W. Bale, E. Bélisle, P. Chartrand, S.A. Decterov, G. Eriksson, A.E. Gheribi, K. Hack, I.H. Jung, Y.B. Kang, J. Melançon, A.D. Pelton, S. Petersen, C. Robelin, J. Sangster, P. Spencer, and M.A. Van Ende, FactSage Thermochemical Software and Databases, 2010–2016, *Calphad*, 2016, **54**, p 35–53
16. M.-A. Van Ende, I.-H. Jung, Y.-H. Kim, and T.-S. Kim, Thermodynamic Optimization of the Dy-Nd-Fe-B System and Application in the Recovery and Recycling of Rare Earth Metals from NdFeB Magnet, *Green Chem.*, 2015, **17**(4), p 2246–2262
17. J. Kim, M.-A. Van Ende, and B. Konar, Thermodynamic Modeling of REE Containing Systems: Energetics of the REE-X Systems (X = Al, Mg, Zn, Si, Sn, Mn, Pb, Fe Co, Ni), *Calphad*, 2015, **51**, p 347
18. I.-H. Jung, M. Sanjari, J. Kim, and S. Yue, Role of RE in the Deformation and Recrystallization of Mg Alloy and a New Alloy Design Concept for Mg-RE Alloys, *Scr. Mater.*, 2015, **102**, p 1–6
19. J. Kim, E. Thibodeau, K. Tetley-Gerard, and I.-H. Jung, Critical Evaluation and Thermodynamic Optimisation of the Sn-RE Systems: Part I. Sn-RE System (RE = La, Ce, Pr, Nd and Sm), *Calphad*, 2016, **55**(2), p 113–133
20. J. Kim and I.-H. Jung, Critical Evaluation and Thermodynamic Optimisation of the Sn-RE Systems: Part II. Sn-RE System (RE = Gd, Tb, Dy, Ho, Er, Tm, Lu and Y), *Calphad*, 2016, **55**(2), p 134–156
21. J. Kim, M. Paliwal, S. Zhou, H. Choi, and I.-H. Jung, Critical Systematic Evaluation and Thermodynamic Optimization of the Mn-RE System (RE = Tb, Dy, Ho, Er, Tm and Lu) with Key Experiments for the Mn-Dy System, *J. Phase Equilib. Diffus.*, 2014, **35**(6), p 670–694
22. J. Kim and I.-H. Jung, Thermodynamic Modelling of Mn-Y and Mn-Gd Systems for Application of RE in Mg Alloy Development, *Can. Metall. Q.*, 2013, **52**(3), p 311–320
23. J. Kim and I.-H. Jung, Critical Systematic Evaluation and Thermodynamic Optimization of the Mn-RE System: RE = La, Ce, Pr, Nd and Sm, *J. Alloys Compd.*, 2012, **525**, p 191–201
24. J. Kim and I.-H. Jung, Critical Evaluation and Thermodynamic Optimization of the Si-RE Systems: Part II. Si-RE System (RE = Gd, Tb, Dy, Ho, Er, Tm, Lu and Y), *J. Chem. Thermodyn.*, 2015, **81**, p 273–297
25. J. Kim and I.-H. Jung, Critical Evaluation and Thermodynamic Optimization of the Si-RE Systems: Part I. Si-RE System (RE = La, Ce, Pr, Nd and Sm), *J. Chem. Thermodyn.*, 2015, **81**, p 253–272
26. M. Zydzik, M. Smids, M.-A. Van Ende, and I.-H. Jung, Critical Thermodynamic Evaluation and Optimization of the Pb-Pr, Pb-Nd, Pb-Tb and Pb-Dy Systems, *Calphad*, 2014, **46**, p 1–17
27. L. Jin, Y.-B. Kang, P. Chartrand, and C.D. Fuerst, Thermodynamic Evaluation and Optimization of Al-Gd, Al-Tb, Al-Dy, Al-Ho and Al-Er Systems Using a Modified Quasichemical Model for the Liquid, *Calphad*, 2010, **34**(4), p 456–466
28. L. Jin, D. Kevorkov, M. Medraj, and P. Chartrand, Al-Mg-RE (RE = La, Ce, Pr, Nd, Sm) Systems: Thermodynamic Evaluations and Optimizations Coupled with Key Experiments and Miedema's Model Estimations, *J. Chem. Thermodyn.*, 2013, **58**, p 166–195
29. Y.-B. Kang, L. Jin, P. Chartrand, A.E. Gheribi, K. Bai, and P. Wu, Thermodynamic Evaluations and Optimizations of Binary Mg-Light Rare Earth (La, Ce, Pr, Nd, Sm) Systems, *Calphad*, 2012, **38**, p 100–116
30. Z. Zhu and A.D. Pelton, Critical Assessment and Optimization of Phase Diagrams and Thermodynamic Properties of RE-Zn Systems—Part II—Y-Zn, Eu-Zn, Gd-Zn, Tb-Zn, Dy-Zn, Ho-Zn, Er-Zn, Tm-Zn, Yb-Zn and Lu-Zn, *J. Alloys Compd.*, 2015, **641**, p 261–271
31. B. Konar, J. Kim, and I.-H. Jung, Critical Systematic Evaluation and Thermodynamic Optimization of the Fe-RE System: RE = La, Ce, Pr, Nd and Sm, *J. Phase Equilib. Diffus.*, 2016, **37**(4), p 438–458
32. A. Pelton, S. Degterov, G. Eriksson, C. Robelin, and Y. Dessureault, The Modified Quasichemical Model I—Binary Solutions, *Metall. Mater. Trans. B*, 2000, **31**(4), p 651–659
33. A.D. Pelton and P. Chartrand, The Modified Quasi-chemical Model: Part II, Multicomponent Solutions, *Metall. Mater. Trans. A*, 2001, **32**(6), p 1355–1360
34. SGTE Data for Pure Elements. (2016). http://www.crct.polymtl.ca/sgte/unary50.tdb
35. H. Kopp, Investigations of the Specific Heat of Solid Bodies, *Philos. Trans. R. Soc. Lond. Ser. A*, 1865, **155**, p 71–202
36. G. Inden, in *Project Meeting CALPHAD V*, (Max-Planck-Institute Eisenforschung, G.m.b.H., Dusseldorf, 1976), p 111
37. M. Hillert and M. Jarl, A Model for Alloying in Ferromagnetic Metals, *Calphad*, 1978, **2**(3), p 227–238
38. M. Hillert, B. Jansson, and B. Sundman, Application of the Compound-Energy Model to Oxide Systems, *Z. Metall.*, 1988, **79**(2), p 81–87
39. Z.-K. Liu, W. Zhang, and B. Sandman, Thermodynamic Assessment of the Co-Fe-Gd Systems, *J. Alloys Compd.*, 1995, **226**(1-2), p 33–45
40. M. Zinkevich, N. Mattern, and H.J. Seifert, Reassessment of the Fe-Gd (Iron-Gadolinum) System, *J. Phase Equilib.*, 2000, **21**(4), p 385–394
41. B. Konar, *Critical Evaluation and Thermodynamic Optimization of the Iron-Rare-Earth Systems* (Department of Mining and Materials, McGill University, Montreal, 2012).
42. O. Kubaschewski, *Iron-Binary Phase Diagrams*, Springer, Berlin, 1982
43. H. Okamoto, Fe-Gd (Iron-Gadolinium), *J. Phase Equilib.*, 1996, **17**(6), p 552
44. M.I. Copeland, M. Krug, C.E. Armantrout, H. Kato, Iron-Gadolinium Phase Diagram, (U.S. Dept. of the Interior, Bureau of Mines, Washington, D.C., 1962)

45. E.M. Savitskii, Rare-Earth Metals, *Metalloved. Term. Obrab. Met. Trans.*, 1961, **9**, p 19–33 (in Russian)
46. E.M. Savitskii, V.F. Terekhova, R.S. Torchinova, I.A. Markova, O.P. Naumkin, V.E. Kolesnichenko, and V.F. Stroganova, Equilibrium Diagram for Alloys of the Gadolinium-Iron System (Les Elements des Terres Rares, Paris-Grenoble, 1969), p 49–60
47. E.M. Savitsij, *Rare Metals and Alloys*, Dom Tekhniki, Moscow, 1959 (Russian)
48. I.V. Burov, V.F. Terekhova, and E.M. Savitskii, Phase Diagrams for States Containing Gadolinium, *Vopr. Teorii i Primeneniya Redkozem. Met. Akad. Nauk SSSR*, 1964, p 116–123
49. S. Atiq, R.D. Rawlings, and D.R.F. West, The Fe-Gd Phase Diagram, *Pak. J. Sci. Ind. Res.*, 2005, **48**(4), p 231–235
50. V.F. Novy, R.C. Vickery, and E.V. Kleber, The Gadolinium-Iron System, *Trans. Am. Inst. Min. Metall. Pet. Eng.*, 1961, **221**, p 580–585
51. I.V. Nikolaenko and V.V. Nosova, Enthalpy of the Mixing of Gadolinium with Manganese and Iron, *Ukr. Khim. Zh. (Russ. Ed.)*, 1989, **55**(12), p 1260–1262
52. M. Ivanov, V. Berezutski, N. Usenko, and N. Kotova, Enthalpies of Mixing in Liquid Alloys of Iron with the Lanthanides, *Int. J. Mater. Res.*, 2013, **104**(9), p 849–857
53. C. Colinet, A. Pasturel, and K.H.J. Buschow, Study of the Enthalpies of Formation in the Gadolinium-(Iron, Cobalt, Palladium, Platinum) Systems, *Metall. Trans. A*, 1987, **18A**(5), p 903–907
54. C. Colinet and A. Pasturel, A Data Base for Enthalpies of Formation of Transition Rare-Earth Metal Alloys, *Calphad*, 1987, **11**(4), p 323–334
55. S.V. Meschel, P. Nash, Q.N. Gao, J.C. Wang, and Y. Du, The Standard Enthalpies of Formation of Some Binary Intermetallic Compounds of Lanthanide-Iron Systems by High Temperature Direct Synthesis Calorimetry, *J. Alloys Compd.*, 2013, **554**, p 232–239
56. S.S. Deodhar and P.J. Ficalora, Reaction Kinetics for the Formation of Rare Earth-Transition Metal Laves Compounds, *Metall. Trans. A*, 1975, **6A**(10), p 1909–1914
57. D.J. Germano, R.A. Butera, and K.A. Gschneidner, Jr., Heat Capacity and Thermodynamic Functions of the RFe_2 Compounds (R = Gd, Tb, Dy, Ho, Er, Tm, Lu) Over the Temperature Region 8 to 300 K, *J. Solid State Chem.*, 1981, **37**(3), p 383–389
58. E. Segal and W.E. Wallace, *Rare Earth Intermetallics*, Academic Press, New York, 1973
59. H. Okamoto, Fe-Tb (Iron-Terbium), *J. Phase Equilib.*, 1996, **17**(2), p 165
60. S. Landin and J. Agren, Thermodynamic Assessment of Fe-Tb and Fe-Dy Phase Diagrams and Prediction of Fe-Tb-Dy Phase Diagram, *J. Alloys Compd.*, 1994, **207-208**, p 449–453
61. M.P. Dariel, J.T. Holthuis, and M.R. Pickus, The Terbium-Iron Phase Diagram, *J. Less-Common Met.*, 1976, **45**(1), p 91–101
62. I.G. Orlova, A.A. Eliseev, G.E. Chuprikov, and F. Rukk, The Fe-Tb System, *Russ. J. Inorg. Chem.*, 1977, **22**(9), p 2557–2562
63. J.L. Chen, G.H. Wu, D.Q. Zhao, S.X. Gao, W.S. Zhan, Y.X. Li, J.P. Qu, and G.Z. Xu, Single-Crystal Growth and Phase Diagram of Tb_2Fe_{17} Compound, *J. Cryst. Growth*, 2001, **222**(4), p 779–785
64. Z.F. Gu, C.F. Xu, D.C. Ao, G. Cheng, X.Q. Gao, Y.S. Du, and L. Ma, Phase Equilibria at 1173 K in the Ternary Fe-Pt-Tb System, *J. Phase Equilib. Diffus.*, 2014, **35**(2), p 163–171
65. D. Gozzi, M. Iervolino, and A. Latini, Thermodynamics of Fe-Rich Intermetallics Along the Rare Earth Series, *J. Chem. Eng. Data*, 2007, **52**(6), p 2350–2358
66. K.H.J. Buschow, Intermetallic Compounds of Rare Earth and 3D Transition Metals, *Rep. Prog. Phys.*, 1977, **40**(10), p 1179–1256
67. H. Okamoto, Dy-Fe (Dysprosium-Iron), *J. Phase Equilib.*, 1996, **17**(1), p 80–81
68. B. Konar, J. Kim, and I.-H. Jung, Thermodynamic Modelling of Fe-Sm and Fe-Dy Systems, *Can. Metall. Q.*, 2013, **52**(3), p 321–328
69. T. Nagai, S. Shirai, and M. Maeda, Thermodynamic Measurement of Dy + Fe Binary System by Double Knudsen Cell Mass Spectrometry, *J. Chem. Thermodyn.*, 2013, **65**, p 78–82
70. A.S. Van der Goot and K.H.J. Buschow, The Dysprosium-Iron System: Structural and Magnetic Properties of Dysprosium-Iron Compounds, *J. Less-Common Met.*, 1970, **21**(2), p 151–157
71. S. Norgren, F. Hodaj, P. Azay, and C. Colinet, Experimental Investigation on the Enthalpies of Formation of the $DyFe_2$, $DyFe_3$, Dy_2Fe_{17}, $ErFe_2$, and $ErFe_3$ Intermetallic Compounds, *Metall. Mater. Trans. A*, 1998, **29A**(5), p 1367–1374
72. T. Nagai, W.-H. Han, and M. Maeda, Thermodynamic Measurement of La-Fe and Y-Fe Alloys by Multi-Knudsen Cell Mass Spectrometry, *J. Alloys Compd.*, 2010, **507**(1), p 72–76
73. H. Okamoto, *Fe-Ho (Iron-Holmium), Phase Diagrams of Binary Iron Alloys*, ASM International, Materials Park, OH, 1993
74. S. Kardellass, C. Servant, N. Selhaoui, A. Iddaoudi, M. Ait Amar, and L. Bouirden, A Thermodynamic Assessment of the Iron + Holmium Phase Diagram, *J. Chem. Thermodyn.*, 2014, **74**, p 78–84
75. G.J. Roe and T.J. O'Keefe, The Fe-Ho Binary System, *Metall. Trans.*, 1970, **1**(9), p 2565–2568
76. T.J. O'Keefe, G.J. Roe, and W.J. James, X-ray Investigation of the Iron-Holmium System, *J. Less-Common Met.*, 1968, **15**(3), p 357–360
77. D.G. Pettifor, Phenomenological and Microscopic Theories of Structure, in S. Sugano, Y. Nishina, S. Ohnishi (Eds.) *Microclusters: Proceedings of the First NEC Symposium, Hakone and Kawasaki, Japan, October 20-23, 1986* (Springer, Berlin, 1987), p 37–46
78. D.G. Pettifor, A Chemical Scale for Crystal-Structure Maps, *Solid State Commun.*, 1984, **51**(1), p 31–34
79. D. Pettifor, New Alloys from the Quantum Engineer, *New Sci.*, 1986, **110**(1510), p 48–53
80. G.J. Zhou, Z.W. Liu, D.C. Zeng, and Z.P. Jin, Thermodynamic Assessment of the Fe-Er System, *Phys. B*, 2010, **405**(17), p 3590–3593
81. A. Meyer, Erbium-Iron System, *J. Less-Common Met.*, 1969, **18**(1), p 41–48
82. K.H.J. Buschow and A.S. Van der Goot, Phase Relations, Crystal Structures, and Magnetic Properties of Erbium-Iron Compounds, *Phys. Status Solidi*, 1969, **35**(1), p 515–522
83. V.E. Kolesnikov, V.F. Trekhova, and E.M. Savitskii, Phase Diagram of the Erbium-Iron System, *Neorg. Mater.*, 1971, **7**(3), p 495
84. H. Okamoto, *Fe-Tm (Iron-Thulium), Phase Diagrams of Binary Iron Alloys*, ASM International, Materials Park, OH, 1993
85. S. Kardellass, C. Servant, N. Selhaoui, and A. Iddaoudi, Thermodynamic Evaluations of the Iron-Lutetium and Iron-Thulium Systems, *Calphad*, 2014, **46**, p 42–54
86. V.E. Kolesnichenko, V.F. Terekhova, and E.M. Savitskii, Phase Diagrams of Thulium-Iron and Lutetium-Iron Alloys, *Metalloved. Tsvet. Metal. Splavov*, USSR, Nauka, Moscow, 1972, p 31–33 (in Russian)
87. E.A. Tereshina and A.V. Andreev, Magnetization and Specific Heat Study of Metamagnetism in Lu_2Fe_{17}-Based Intermetallic Compounds, *Intermetallics*, 2010, **18**(6), p 1205–1210
88. K.A. Gschneidner, Jr., *Rare Earth Alloys*, D. Van Nostrand Co., New York, 1961, p 186
89. B.W. Zhang, G. Liu, and K. Han, The Fe-Y (Iron-Yttrium) System, *J. Phase Equilib.*, 1992, **13**(3), p 304–308
90. Z. Du, W. Zhang, and Y. Zhuang, Thermodynamic Assessment of the Fe-Y System, *Rare Met. (Beijing)*, 1997, **16**(1), p 52–58

91. D. Lü, C. Guo, C. Li, and Z. Du, Thermodynamic Description of Fe-Y and Fe-Ni-Y Systems, *Phys. Procedia*, 2013, **50**, p 383–387
92. S. Kardellass, C. Servant, N. Selhaoui, A. Iddaoudi, M.A. Amar, and L. Bouirden, A Thermodynamic Assessment of the Iron-Yttrium System, *J. Alloys Compd.*, 2014, **583**, p 598–606
93. M.S. Farkas and A.A. Bauer, The Solid Solubility and Constitution of Yttrium in Iron-20 to 40 w/o Chromium Alloys, in *USAEC Report* (1959), p 20
94. R.F. Domagala, J.J. Rausch, and D.W. Levinson, The Systems Y-Fe, Y-Ni, and Y-Cu, *Trans. Am. Soc. Met.*, 1961, **53**, p 137–155
95. L. Li and Z. Xing, Solubilities of Ce, Nd and Y in α-Fe, *Jinshu Xuebao*, 1993, **29**(3), p A136–A141
96. G.M. Ryss, Y.O. Esin, M.S. Petrushevskii, A.I. Stroganov, and P.V. Gel'd, Effect of Short-Range Order on the Enthalpies of Formation of Molten Alloys of Iron with Yttrium, *Izv. Vyssh. Uchebn. Zaved. Chern. Metall.*, 1977, **8**, p 9–12
97. V.S. Sudavtsova, V.P. Kurach, and G.I. Batalin, Thermochemical Properties of Molten Binary Fe-(Y, Zr, Nb, Mo) Alloys, *Russ. Metall. Metally*, 1987, **3**, p 59–60
98. H.H. Van Mal, K.H.J. Buschow, and A.R. Miedema, Hydrogen in Metals Hydrogen Absorption of Rare-Earth (3D) Transition Intermetallic Compounds, *J. Less-Common Met.*, 1976, **49**, p 473–475
99. L.H. Bennett and R.E. Watson, A Database for Enthalpies of Formation of Binary Transition Metal Alloys, *Calphad*, 1981, **5**(1), p 19–23
100. P.R. Subramanian and J.F. Smith, Thermodynamics of Formation of Yttrium-Iron Alloys, *Calphad*, 1984, **8**(4), p 295–305
101. M.P. Dariel, U. Atzmony, and R. Guiser, Specific Heat Anomalies at the Magnetic Ordering Temperatures of Rare Earth-Iron Laves Compounds, *J. Less-Common Met.*, 1974, **34**(2), p 315–319
102. K. Mandal, A. Yan, P. Kerschl, A. Handstein, O. Gutfleisch, and K.H. Mueller, The Study of Magnetocaloric Effect in R_2Fe_{17} (R = Y, Pr) Alloys, *J. Phys. D Appl. Phys.*, 2004, **37**(19), p 2628–2631
103. K. Takeda, T. Maeda, and T. Katayama, Temperature Dependence of the Magneto-crystalline Anisotropy in R_2Fe_{17} (R = Y, Gd, Tb, Dy, Er), *J. Alloys Compd.*, 1998, **281**(1), p 50–55
104. P.I. Kripyakevich, D.P. Frankevich, and Y.V. Voroshilov, Compounds with Structures of the Th_6Mn_{23} Type in Alloys of Rare Earth Metals with Mn and Fe, *Poroshk. Metall. (Kiev)*, 1965, **5**(11), p 55–61
105. M.H. Nguyen, J.J.M. Franse, and P.T. Nguyen, Magnetic Anisotropy of the Yttrium-Cobalt-Iron ($Y(Co_{1-x}Fe_x)_3$) Pseudobinary Compounds, *J. Magn. Magn. Mater.*, 1989, **80**(2-3), p 159–164
106. J.A. Chelvane and G. Markandeyulu, Magnetic Properties of $Y_{1-x}Gd_xFe_2B_y$[x = 0, 0.25, 0.5, 0.75, 1; y = 0, 0.1, 0.15, 0.2], *J. Alloys Compd.*, 2006, **421**(1-2), p 35–41
107. S. Kardellass, C. Servant, N. Selhaoui, A. Iddaoudi, M. Ait Amari, and L. Bouirden, Thermodynamic Assessments of the Fe-Y and Ni-Sc Systems, in *MATEC Web of Conferences* (2013), p 01008
108. H.R. Kirchmayr, Magnetic Properties of the Compound Series $Y(Mn_xFe_{1-x})_2$ and $Y_6(Mn_xFe_{1-x})_{23}$, *J. Appl. Phys.*, 1968, **39**(2), p 1088–1089
109. W. He, X. Wang, J. He, J. Wen, M. Yu, and L. Zeng, Isothermal Section of the Y-Fe-Cr Ternary System at 773 K, *J. Alloys Compd.*, 2010, **502**(1), p 87–91
110. A.R. Miedema, P.F. de Châtel, and F.R. de Boer, Cohesion in Alloys-Fundamentals of a Semi-empirical Model, *Phys. B + C*, 1980, **100**(1), p 1–28
111. A.R. Miedema, A.K. Niessen, F.R. De Boer, R. Boom, and W.C.M. Matten, *Cohesion in Metals: Transition Metal Alloys*, North-Holland, Amsterdam, 1989
112. R.F. Zhang and B.X. Liu, Proposed Model for Calculating the Standard Formation Enthalpy of Binary Transition-Metal Systems, *Appl. Phys. Lett.*, 2002, **81**(7), p 1219–1221
113. R.F. Zhang and B.X. Liu, Thermodynamic Criterion for the Formation of Laves Phases in Binary Transition-Metal Systems, *Philos. Mag. Lett.*, 2005, **85**(6), p 283–287
114. R.F. Zhang, S.H. Sheng, and B.X. Liu, Predicting the Formation Enthalpies of Binary Intermetallic Compounds, *Chem. Phys. Lett.*, 2007, **442**(4-6), p 511–514
115. S.K. Malik, T. Takeshita, and W.E. Wallace, Effects of Absorbed Hydrogen on the Magnetic Properties of Gadolinium-Iron ($GdFe_3$), Dysprosium-Iron ($DyFe_3$) and Holmium-Iron ($HoFe_3$), *Magn. Lett.*, 1976, **1**(2), p 33–39
116. S. Barth, E. Albert, G. Heiduk, A. Moeslang, A. Weidinger, E. Recknagel, and K.H.J. Buschow, Local Magnetic Fields in Ferromagnetic Intermetallic Compounds of Cubic Laves-Phase Type, *Phys. Rev. B Condens. Matter*, 1986, **33**(1), p 430–436
117. S.K. Malik, F. Pourarian, and W.E. Wallace, Magnetization Behavior of RFe_3-Hydrides (R = Tb, Er and Tm), *J. Magn. Magn. Mater.*, 1983, **40**(1-2), p 27–31
118. J.J. Bara, A.T. Pędziwiatr, W. Zarek, D. Konopka, and U. Gacek, Investigations of $Dy(Fe_xAl_{1-x})_2$ Laves Phases by X-ray, Magnetometric and Mössbauer Effect Methods, *J. Magn. Magn. Mater.*, 1982, **27**(2), p 159–167
119. Y.Q. Chen, J.K. Liang, J. Luo, J.B. Li, and G.H. Rao, Anomalous Phase Composition in the Two-Phase Region of $DyFe_{3-x}Al_x$ ($x \leq 1.0$), *Powder Diffr.*, 2010, **25**(04), p 349–354
120. Y. Zhuang, W. Qin, and H. Zhou, The 500 °C Isothermal Section of the Phase Diagram of the Ternary Ho-Fe-Nb System, *J. Alloys Compd.*, 1997, **248**(1-2), p 206–208
121. A.T. Pedziwiatr, H.K. Smith, and W.E. Wallace, Magnetic and Structural Characteristics of Ho_6Fe_{23} Deuterides, *J. Solid State Chem.*, 1983, **47**(1), p 41–46
122. Y.V. Knyazev, Y.I. Kuz'min, A.G. Kuchin, A.V. Lukoyanov, and I.A. Nekrasov, Sm_2Fe_{17} and Tm_2Fe_{17}: Electronic Structure, Magnetic and Optical Properties, *J. Phys. Condens. Matter*, 2007, **19**(11), p 116215
123. O. Isnard, S. Miraglia, J.L. Soubeyroux, D. Fruchart, and P. l'Heritier, A Structural Analysis and Some Magnetic Properties of the $R_2Fe_{17}H_x$ Series, *J. Magn. Magn. Mater.*, 1994, **137**(1-2), p 151–156